HALL-BROWN, MARY, Ph.D. The EO-1 Hyperion and Advanced Land Imager Sensors for use in Tundra Classification Studies within the Upper Kuparuk River Basin, Alaska. (2012)
Directed by Dr. Roy S. Stine, 120 pp.

The heterogeneity of Arctic vegetation can make land cover classification very difficult when using medium to small resolution imagery (Schneider et al., 2009; Muller et al., 1999). Using high radiometric and spatial resolution imagery, such as the SPOT 5 and IKONOS satellites, have helped Arctic land cover classification accuracies rise into the 80 to 90 percentiles (Allard, 2003; Stine et al., 2010). However, those increases usually come at a high price. High resolution imagery is very expensive and can often add tens of thousands of dollars into the research. The EO-1 satellite launched in 2002 carries two sensors that have high spectral and/or high spatial resolutions and can be an acceptable compromise between the resolution-versus-cost issues. The Hyperion is a hyperspectral sensor with the capability of collecting 242spectral bands of information. The Advanced Land Imager (ALI) is an advanced multispectral sensor with a spatial resolution that can be sharpened to 10 meters. This dissertation compares the accuracies of Arctic land cover classifications produced by the Hyperion and ALI sensors to the classification accuracies of the Système Pour l'Observation de le Terre (SPOT) and Landsat TM and ETM+ sensors.

Hyperion and ALI images from August 2004 were collected over the Upper Kuparuk River Basin, Alaska. Image processing included the stepwise discriminant analysis of pixels that were positively classified from coinciding ground control points, geometric and radiometric correction, and principle component analysis. Finally

stratified random sampling was used to perform accuracy assessments on satellite derived land-cover classifications.

Accuracy was estimated from an error matrix (confusion matrix) that provided the overall, producer's and user's accuracies. This research found that while the Hyperion sensor produced classification accuracies that were equivalent to the TM and ETM+ sensors (approximately 78%) the Hyperion could not obtain the accuracy of the SPOT 5 HRV sensor. However, the land cover classifications derived from the ALI sensor exceeded most classification accuracies derived from the TM and ETM+ sensors and were even comparable to most SPOT 5 HRV classifications (87%).

With the deactivation of the Landsat series satellites, the monitoring of remote locations such as in the Arctic on an uninterrupted basis throughout the world is in jeopardy. The utilization of the Hyperion and ALI sensors are a way to keep that endeavor operational. By keeping the ALI sensor active at all times, uninterrupted observation of the entire Earth can be accomplished. Keeping the Hyperion sensor as a "tasked" sensor can provide scientists with additional imagery and options for their studies without overburdening storage issues.

THE EO-1 HYPERION AND ADVANCED LAND IMAGER SENSORS FOR USE IN TUNDRA CLASSIFICATION STUDIES WITHIN THE UPPER KUPARUK RIVER BASIN, ALASKA

by

Mary Hall-Brown

A Dissertation Submitted to
the Faculty of The Graduate School at
The University of North Carolina at Greensboro
in Partial Fulfillment
of the Requirements for the Degree
Doctor of Philosophy

Greensboro
2012

Approved by

Dr. Roy Stine
Committee Chair

To my family

Walsteen and Mary Hall

Michael, Skyler, and Jordan Brown

Nancy, Lynn, Vicky, Buddy, and Caro Hall

APPROVAL PAGE

This dissertation has been approved by the following committee and the Faculty of the Graduate School at the University of North Carolina Greensboro.

Committee Chair Dr.Roy Stine

Committee Members Dr. Anne Hershey

Dr. Zhi-Jun Liu

Dr. Rick Bunch

_____
Date of Acceptance by Committee

08/08/2012
Date of Final Oral Examination

ACKNOWLEDGEMENTS

I would like to thank my chairman and his wife, Drs. Roy and Linda Stine, for their support and encouragement, without which I could not have finished. They have been supportive throughout this process and I will never be able to thank them enough. I would also like to thank my committee, Dr. Zhi-Jun Liu, Dr. Rick Bunch, and Dr. Anne Hershey for their input, leadership, and patience. I would especially like to thank Dr. Hershey for providing the majority of the funding for my visits to the research site near Toolik Lake, Alaska. I would also like to thank Drs. Chris Lueke, Steve Whalen, John O'Brian and the personnel at Toolik Field Research Station, Alaska for the kindness and support they provided.

I would also like to thank Dr. Prasad Pathak, Dr. Debashish Chaudhri, Leanne Sulewski, Robert Northington and Cassidy Hey not only for their assistance in the field and technical expertise in the lab (and willingness to share said expertise), but also for their support and friendship.

I would finally like to say to my family, Jordan, Skyler and Michael Brown, and to friends who have become family, Jeff Patton, Gordon Bennett, Jim and Liz Nelson, Selima Sultana and Mich Ciapanna, thank you all for the never ending encouragement, support and wisdom you each offered. For his assistance with crazy computer issues, I want to specifically thank Jim Nelson.

This research is one of several sponsored by the National Science Foundation grant, “The Geomorphic-Tropic Hypothesis (GTH) Research for Benthic-Pelagic Coupling in Arctic Lakes”.

TABLE OF CONTENTS

Page

LIST OF TABLES

Page

LIST OF FIGURES

Page

ACRONYMS

AMAP	Arctic Monitoring and Assessment Programme
ALI	Advanced Land Imager
ACIA	Arctic Climate Impact Assessment
AOI	Area of Interest
BV	Brightness Value
DOS	Dark Object Subtraction
EOS	Earth Observing Satellite
ERDAS	Earth Resource Data Analysis System
EMR	Electromagnetic Radiation
EROS	Earth Resources Observation and Science
ERTS	Earth Resources Technology Satellite
ESRI	Environmental Systems Research Institute
ETM	Enhanced Thematic Mapper
GCP	Ground Control Point
GIS	Geographic Information Science
GPS	Global Positioning System
HRV	High Resolution Visible
ISODATA	Iterative Self-Organizing Data Analysis
LIDAR	Light Detection and Ranging
NASA	National Aeronautic Space Agency

NDVI	Normalized Difference Vegetative Index
NOAA	National Oceanic and Atmospheric
SPOT	Système Pour l'Observation de la Terre
SAR	Synthetic Aperture Radar
SPOT	Système Pour l'Observation de le Terre
SWIR	Short Wave Infrared
UKRB	Upper Kuparuk River Basin
USDA	United States Department of Agriculture
UTM	Universal Transverse Mercator
WGS	World Geodetic System

CHAPTER I

INTRODUCTION

1.1 Arctic Environment

The Arctic is often defined by its geographic position as well as its land cover characteristics. The Arctic Monitoring and Assessment Programme (AMAP) has defined the Arctic as "the terrestrial and marine areas north of the Arctic Circle (66°32'N), and north of 62°N in Asia and 60°N in North America, modified to include the marine areas north of the Aleutian chain, Hudson Bay, and parts of the North Atlantic Ocean including the Labrador Sea" (AMAP, 2003, 1). The National Snow and Ice Data Center defines the Arctic as

> The southern limit of the Arctic region is commonly placed at the Arctic Circle (latitude 66 degrees, 32 minutes North). The Arctic Circle is an imaginary line that marks the latitude above which the sun does not set on the day of the summer solstice (usually 21 June) and does not rise on the day of the winter solstice (usually 21 December). North of this latitude, periods of continuous daylight or night last up to six months at the North Pole (NSICD, 2012, 1).

Geographic position and land cover characteristics are only two ways of describing the Arctic. Geological and environmental information can also provide important characteristics of the Arctic's definition.

Within the Arctic region of Alaska the North Slope is a large expanse of wilderness rich in resources and history. Carbonate rich marine rocks created during the

early to mid-Paleozoic Era dominate the North Slope and the Brooks Range subterraneous geology. They are a testament to the region's evolution from sea floor to terra firma. There are two major orogenic events-- the Ellesmerian (early Mississipian and older strata) and the Brookonian event (middle Jurassic to Early Cretaceous), and several minor orographic events. Non-marine to shallow marine clastic rocks such as sandstones, conglomerates, shales, and mudstones begin to appear in the rock record of the North Slope during the Mesozoic Era. The surficial deposits of the North Slope are consecutive layers of glacial till, alluvium, and gravels that were laid down from cyclical glaciation events of the Cenozoic Era (Moore et al., 1994; Hamilton, 1978 & 2002). As glacial events modified the North Slope, a complex landscape emerged encompassing small glacial lakes with interconnected rivers which dominate the landscape, along with their coinciding deposits of lacustrine, alluvium, and colluvium (Hamilton, 2002; Moore et al., 1994). The vegetation patterns and assemblages present on Alaska's North Slope are thought to be a direct response of this glacial landscape (Bockheim et al, 1998; Riedel et al., 2005; Walker et al. 1987; Walker et al, 2005).

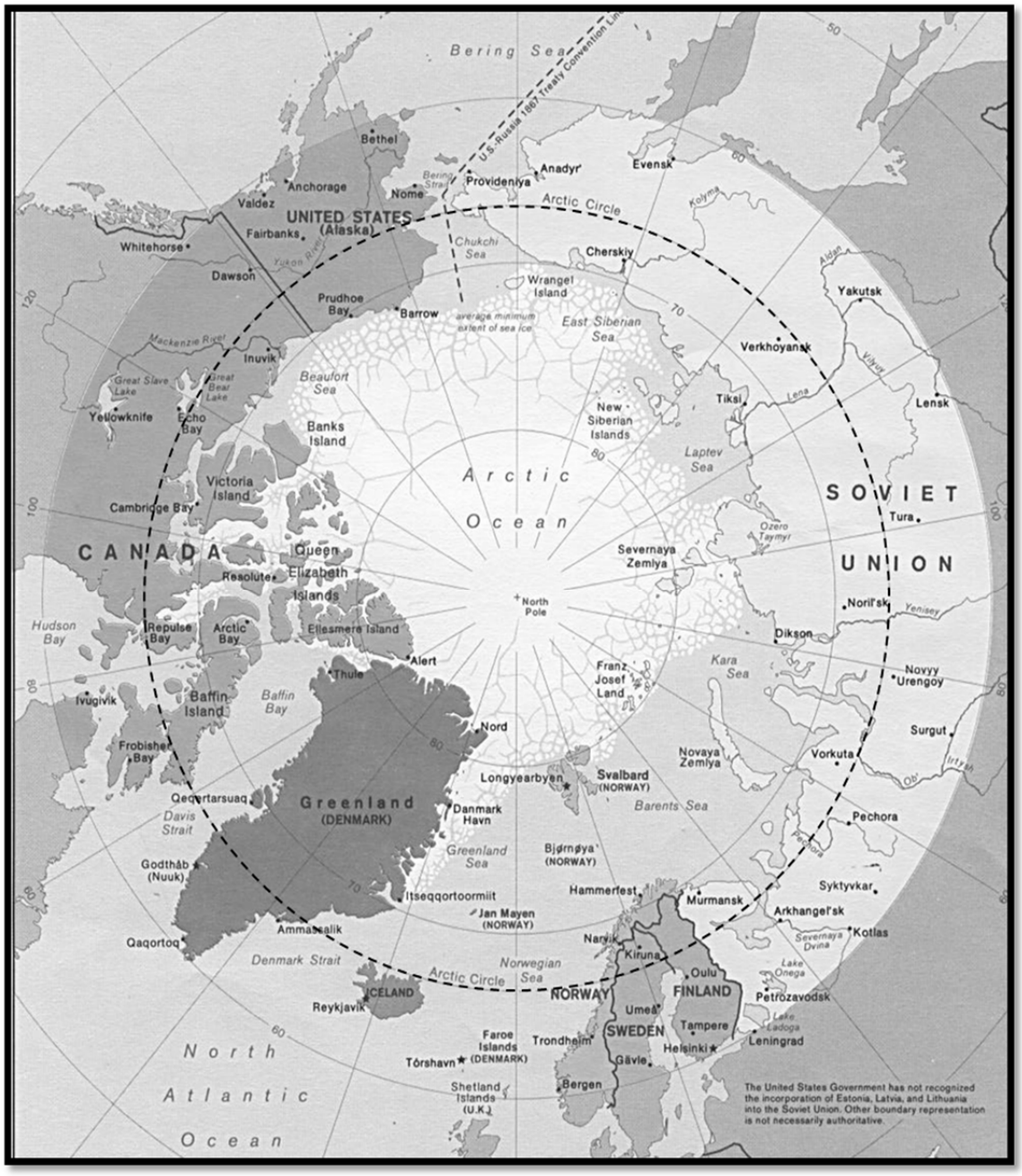

Figure 1.1 Arctic Region, CIA 1987.
From the Perry-Castañeda Library Map Collection at University of Texas at Austin

.

1.2 Warming Arctic Environment

According to the Arctic Climate Impact Assessment, the Arctic region is warming at twice the global average (ACIA, 2005). Twenty years ago, researchers attempting to predict the effects of climate change on ecosystems worldwide were facing the reality that the "knowledge of the structure and functioning of terrestrial ecosystems on a global scale" (Mooney, 1991, p. 112) was not understood well enough to use them to predict what consequences climate change would have on the terrestrial systems or subsequent atmospheric interactions. Mooney stated that in order to understand these ecosystems and their "changing nature" (p. 112) new assessment tools were needed as well as long term and large-scale ecosystems studies: (Mooney, 1991). While Mooney believes the Arctic's response to warming will be "limited" (Mooney, 1991, p. 116) due to low temperatures and low nutrient availability, others disagree. In Nature magazine only two months later, the Arctic is labeled a "bellwether" (Walsh, 1991:19) for climate change.

It has been estimated that "one-third of the total world pool of soil carbon" is within the Northern latitudes (Gorham, 1991, p.183). Permafrost soils extend throughout the Arctic and store vast amounts of organic matter (OM) within their layers. Previously frozen soils will start to thaw and release an ever increasing volume of CH_4 (methane) and CO_2 (Carbon Dioxide) into the atmosphere (Figure 1.2) as warming temperatures permeate deeper within the ground. As Arctic temperatures warm and release carbon, a positive feedback cycle will be created that will have a global impact that will contribute to further warming. The warming temperatures will have a furthering effect on

vegetation boundaries and species (Chapin et al., 2005; Sitch et al., 2007; Comiso, 2003, 2006).

The following is an excerpt from the Arctic Report Card (2007) which describes how vegetation boundaries respond to warming temperatures.

> In northern latitudes, there is a series of vegetation and plant life form boundaries that are associated with temperature. They generally move northwards as climate becomes warmer although advance is not expected to be uniform, in part due to differences in individual species response. The latitudinal treeline is the most obvious one, and is associated with the isotherm for July mean monthly temperature of about 11° C. North of this boundary, one finds the shrubline, and further north, the tundra becomes completely devoid of woody plants. Along this latitudinal gradient, the height of the vegetation decreases, the complexity of the plant canopy is reduced and the biodiversity generally decreases. There also tends to be a decrease in the carbon annually captured by photosynthesis and an increase in albedo (i.e. the incoming solar radiation reflected from the land surface). As the latitudinal distribution of plant life forms are associated with climate, vegetation zone dynamics and shifts in their composition are considered one of the major processes that will respond to a warming Arctic (Callaghan et al., 2004a) (p32).

Previous and ongoing research is providing a better understanding and appreciation of the Arctic ecosystem. Technological advancements during this time have also brought about remarkable advancements in the acquisition, storage, and analysis of spatial data.

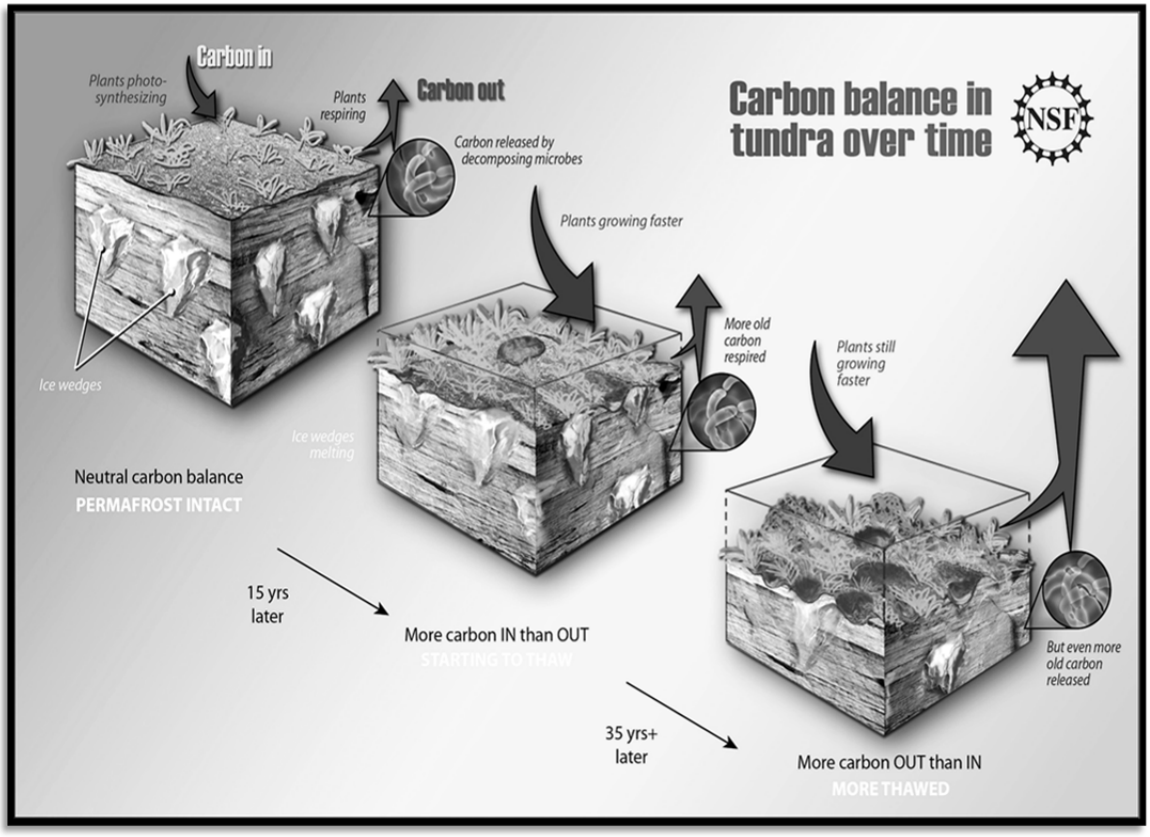

Figure 1.2 Warming Arctic climate will aid the release of an ever increasing amount of carbon. (Zina Deretsky, National Science Foundation)

1.3 Remote Sensing Essentials

Remote sensing can be defined as "the acquisition of information about the state and condition of an object through sensors that are not in physical contact with it" (Chuvieco and Huete, 2010:1). There are two types of optical sensors used in remote sensing; active and passive. An active sensor not only records energy wavelengths but transmits them as well (i.e. sonar, radar). Passive sensors only record electro-magnetic-radiation (EMR) that is emitted or reflected by features themselves (i.e. sunlight reflecting off vegetation) (Figure 1.2). Information recorded by the sensor is converted to

digital numbers (DN) and formatted into a 2-D cell array (Figure 1.3) that will represent the feature's optical properties and is used for identification and classification purposes (Jensen, 2004; Chuvieco and Huete, 2010). The remote sensing process "involves an interaction between incident radiation [sunlight] and the targets of interest" (CCRS, 2008, p. 1). Sensors vary in purpose and platform so their optical specifications will vary as well, and their imagery will incorporate varying characteristics.

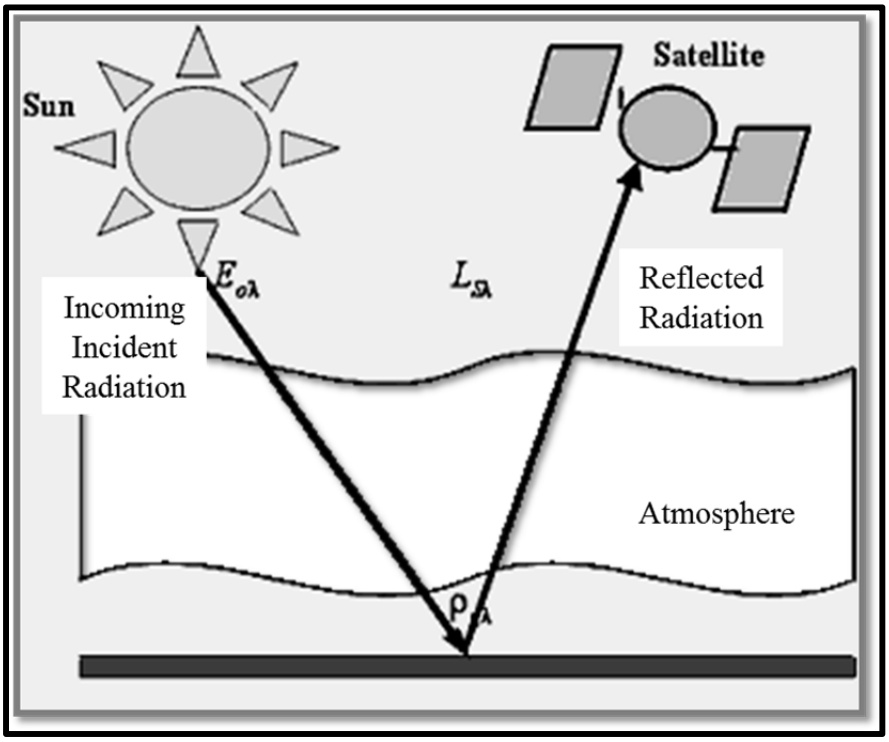

Figure 1.3 Diagram of radiant energy.
(http://www.ars.usda.gov/Main/docs.htm?docid=10306&pf=1&cg_id=0)

An image integrates four types of resolution: spatial, spectral, radiometric, and temporal. Spatial resolution represents the finest (minimum) unit of information (pixel) to which detail can be obtained (i.e. 30m). Spectral resolution delineates areas

(bandwidths) within the EMR spectrum (Appendix A) that are recorded by the sensor. More bands will provide greater detail. The radiometric resolution determines a sensors' ability to discriminate slight energy levels (sensitivity). For example, an 8-bit sensor can discriminate 256 levels of energy while a 16-bit sensor discriminates 65,536. Finally, the temporal resolution (or revisit time) of a sensor indicates the time required for a sensor to reimage the same location (Jensen, 2004; Huvieco and Huete, 2010). Resolution specifications for sensors utilized within this study are listed in Table 1.

Table 1. Sensor Resolution Specifications. (Avery & Berlin, 1992; NASA, 2011)

Sensor	**Resolution**			
	Spatial	Spectral	Radiometric	Temporal
SPOT	5m	4	8	8 days
Thematic Mapper	30m	7	8	16 days
Enhanced Thematic Mapper	30m	7	8	16 days
ALI	30m	10	16	16 days
HYPERION	30m	242	16	16 days

1.4 Problem Definition

Research by conventional methods within the Arctic is not only spatially limiting, but it is also time consuming and expensive. The inaccessibility of much of the Arctic landscape is a major problem for most Arctic researchers. Accessibility problems include limited and expensive transportation options to reach study sites, limited time span of warmer temperatures, study sites may cover large expanses and incorporate difficult terrain, and also, abruptly changing weather. Additional complications for remote sensing image acquisition within the Arctic include lingering snow and ice cover, the heterogeneity of Arctic vegetation, greater levels of cloud cover during summer months, a satellite's revisit time, short growing season, and solar zeniths (Stow et al., 2004).

Non-site specific complications for remote sensing can include diminished or damaged imagery, sensor variations (calibration differences), the loss or lack of documentation (environmental conditions present when image is acquired), or partial to complete satellite failure (Miller, 1973; Walker et al., 1982 and 1987; Muller et al., 1998; Nagendra and Gadgil, 1999; Jia, 2003; and Stow et al., 2003). In 2003, the scan line corrector (SLC) on the Landsat 7 ETM+ sensor failed causing the loss of approximately 25% of the entire image area (USGS, 2006).

Medium to high resolution imagery can be obtained at little or no cost through local government agencies or web sites such as Google Earth™[1] or Terralook™[2] as long

[1] Google Earth is a product of Google Inc.

as the research area is within or near one of Alaska's larger cities. Outside of the larger cities, however, the costs involved to overcome some of these Arctic-related problems can be enormous. For researchers with areas in remote regions of Alaska, obtaining current high radiometric and spatial resolution imagery (satellite or aerial photographs) can be very prohibitively expensive.

To overcome these cost limitations, Arctic researchers have primarily relied on the free or inexpensive Landsat, Moderate Resolution Infrared Spectrometer (MODIS), IKONOS and/or the Advanced Very High Radiometric Radiometer (AVHRR) satellite imagery to use within their studies (Walker et al., 1994; Stow et al., 2000, 2003, 2004; Frohn et al., 2005; Hope et al., 2003; Hirtle and Rencz, 2003; Jia et al., 2003, 2006; Kimball et al., 2006; Muller et al., 1998; Sturm et al., 2001; Steinberg et al., 2006, Tape et al., 2006; Tucker et al., 2001).

Even with these challenges, numerous Arctic scientists still choose to work with imagery datasets because of the potential data that may be added to their research. Recent technological and image processing advancements (discussed in chapters 2 and 3) can help address many of these Arctic specific issues that researchers face as they work to gain a better understanding of the Arctic region.

---

[2] TerraLook collections, a joint NASA and USGS product, are distributed by USGS/EROS, Sioux Falls, SD and consist of data from USGS/EROS and the NASA Land Processes Distributed Active Archive Center (LP DAAC).

1.5 Research Objectives

The objectives of this study are

1. Compare the optical properties of various Arctic land covers as derived from four satellite sensors: the multispectral ETM+, the advanced multispectral ALI, the hyperspectral Hyperion, and the multispectral (high resolution) SPOT.
2. Identify the sensor producing highest accuracy land cover classification
3. Identify the land cover type most accurately recognized
4. Provide additional methods to utilize Hyperion and ALI imagery in Arctic studies
5. Provide further discourse for the evolution of data continuity between Landsat and EO-1 sensors and previous Arctic studies.

The research proposed in this study adds to the scientific knowledge of Arctic environments by investigating the use and contributions of hyperspectral and advanced multispectral remote sensing technologies.

1.6 Research Question

Specifically, this research seeks to answer if the enhanced radiometric and spectral sensitivity of the Hyperion and ALI sensors can be used to generate Arctic land cover classifications with comparable or higher accuracy rates than those produced by the Landsat TM and ETM+ sensors as well as the higher spatial resolution, and much more expensive, SPOT 5 sensor.

1.7 Dissertation Structure

This dissertation is divided into five chapters. Chapter 1, the present chapter, provides the basis and justification for this research. Chapter 2 provides the literature review and a small discourse on basic remote sensing technical and methodological aspects. It also lays the foundation for this dissertation's research through presentation of previous Arctic research involving satellite imagery. Chapter 3 introduces the study area and data and discusses the methodology used to achieve the aforementioned research goals. Chapter 4 describes the results ascertained from this research. Finally, chapter 5 summarizes the major findings, as well as illustrates limitations of the study, and highlights the need for future work.

CHAPTER II

LITERATURE REVIEW

2.1 Utilizing Remote Sensing in Arctic Research

Research by conventional methods within the Arctic is not only spatially limited but also time-consuming and expensive. Over the past three decades, various scientific disciplines have increasingly incorporated remote sensing components into their studies in the Arctic (Miller, 1973; Spjelkavik, 1995; Muller, 1998; Nagendra and Gadgil, 1999; Jia, 2003; and Stow et al., 2003). Remote sensing has been used to create time-change analysis (Rees et al., 2003; Tommercik et al., 2003), identify critical habitat (Frohn et al., 2005; Theau et al., 2005; Belchansky et al., 1995), create sampling strategies (Shiklomanov and Nelson, 2002), quantify methane emissions (Schneider et al., 2009), identify phenological trends (Olthof and Latifovic, 2007), quantify glacier retreat rates (Bishop et al., 1998; Cullen et al., 2006), and monitor permafrost loss (Hinkel et al., 2007; Tutubalina and Rees, 2001), as well as many other research projects. Changes in the Arctic environment due to climate warming have become a primary focus for much of the ongoing Arctic research: identification, assessment, and environmental monitoring (McDonald et al., 1996; Verbyla, 2008; Kimball et al., 2008; Zoran & Stefan, 2006; Vourlitis et al., 2003). Utilizing the latest remote sensing technology provides Arctic researchers the opportunity to increase their research areas, reduce field time, and, depending on the scale of the study, reduce overhead costs. The incorporation of remote

sensing into a research agenda can also help offset difficulties inherent with any type of Arctic study such as a short growing season, traversing large distances over difficult terrain, and abruptly changing weather (Stow et al., 2004). While accuracy rates for identification or classification based solely on imagery are slightly lower than those based solely on field observations, the combination of the two may provide acceptable accuracy rates for researchers wanting to study larger extents without sacrificing much detail. GIS and remote sensing technologies allow researchers to collect data from places that were previously thought too difficult or dangerous to traverse. These technologies make data acquisition, storage, and analysis much less difficult and time consuming. They even give researchers the capacity to distribute data much sooner and with greater ease. The combination of ground studies and remote sensing technologies may become the standard for the next generation of Arctic researchers. However, as previously mentioned, there are intrinsic complications for studies of any kind in the Arctic Circle, and remote sensing is certainly no exception. Complications for image acquisition include 1) lingering snow and ice cover, 2) heterogeneity of Arctic vegetation, 3) cloud cover, 4) satellite revisit time, 5) short growing season, and 6) solar zeniths (Stow et al., 2004).

In the past twenty to thirty years, the Northern Slope of Alaska has been home to numerous scientific studies focusing on biological, climatological, geological, and limnological topics (Walker, 1987; McDonald et al., 1996; Hamilton, 2002). While many of the more recent studies investigate environmental change attributed to warming temperatures (Epstein et al., 2004; Stow et al., 2004; Nordberg, 2003; Tommervik et al., 2003; Olthof and Latifovic, 2007), initial research using satellite imagery was primarily

directed towards Arctic land cover and natural resource identification, classification, and mapping (Walker et al., 1987; Walker & Acevedo, 1987; Miller, 1973; George et al., 1977; Gorham, 1991; and Fleming & Talbot, 1982).

2.2 Sensor Specification and Evolution

Over the past three decades, the Landsat Satellite series (Figure 2.1), originally named ERTS (Earth Resources Technology Satellite), was the source for much of the image-based research performed within the Arctic (Miller, 1973; George et al., 1976; Fleming et al., 1982; Walker et al., 1982, 1987, 1994). Environmental resource and land cover mapping was performed using some of the first images available from the satellite (Miller, 1973; Walker et al., 1982, 1987). Studies using the Multispectral Sensor (MSS) on Landsat 1 through 3, with its coarse spatial (80 meters) and spectral sensitivity (four bands), had to be at small regional scales and not the large local scales at which most researchers worked (NASA, 20011).

Landsat 5, deployed in 1984, carried an improved sensor, the Thematic Mapper (TM). The spatial resolution was still 30 meters, but the spectral resolution was increased to seven bands. Landsat 5, only recently taken out of operation, provided the lion's share of imagery for Arctic research (Liston et al., 2002; Olthof & Latifovic, 2007; Stow et al., 2004; Tommervick et al., 2003; Nordberg; 2003; Walker et al., 1993; Verbyla, 2008; Epstein et al., 2004; Jia et al., 2006; Riedel et al., 2009; Gratto-Trevor, 1996; Théau et al., 2005). Landsat 6 was launched on October 5th, 1993 but failed to achieve orbit. When Landsat 7 deployed in 1999, it carried an enhanced version of the Thematic Mapper

(ETM+). The ETM+ sensor included a pan band (15 meters) that doubled the Landsat spatial resolution. Unfortunately, the scan line corrector failed on the sensor in 2003 causing large stripes that carry no data. Only the small area directly beneath the sensor (NADIR) is unaffected by the failure (NASA, 2011) (Figure 2.2).

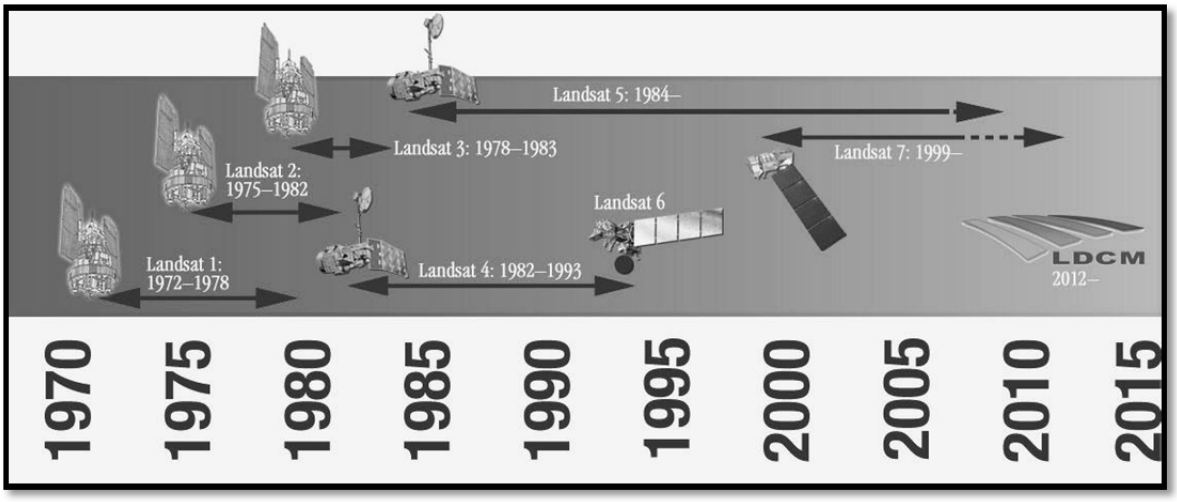

Figure 2.1 Landsat time line.
(http://landsat.gsfc.nasa.gov/graphics/timeline-lg.jpg)

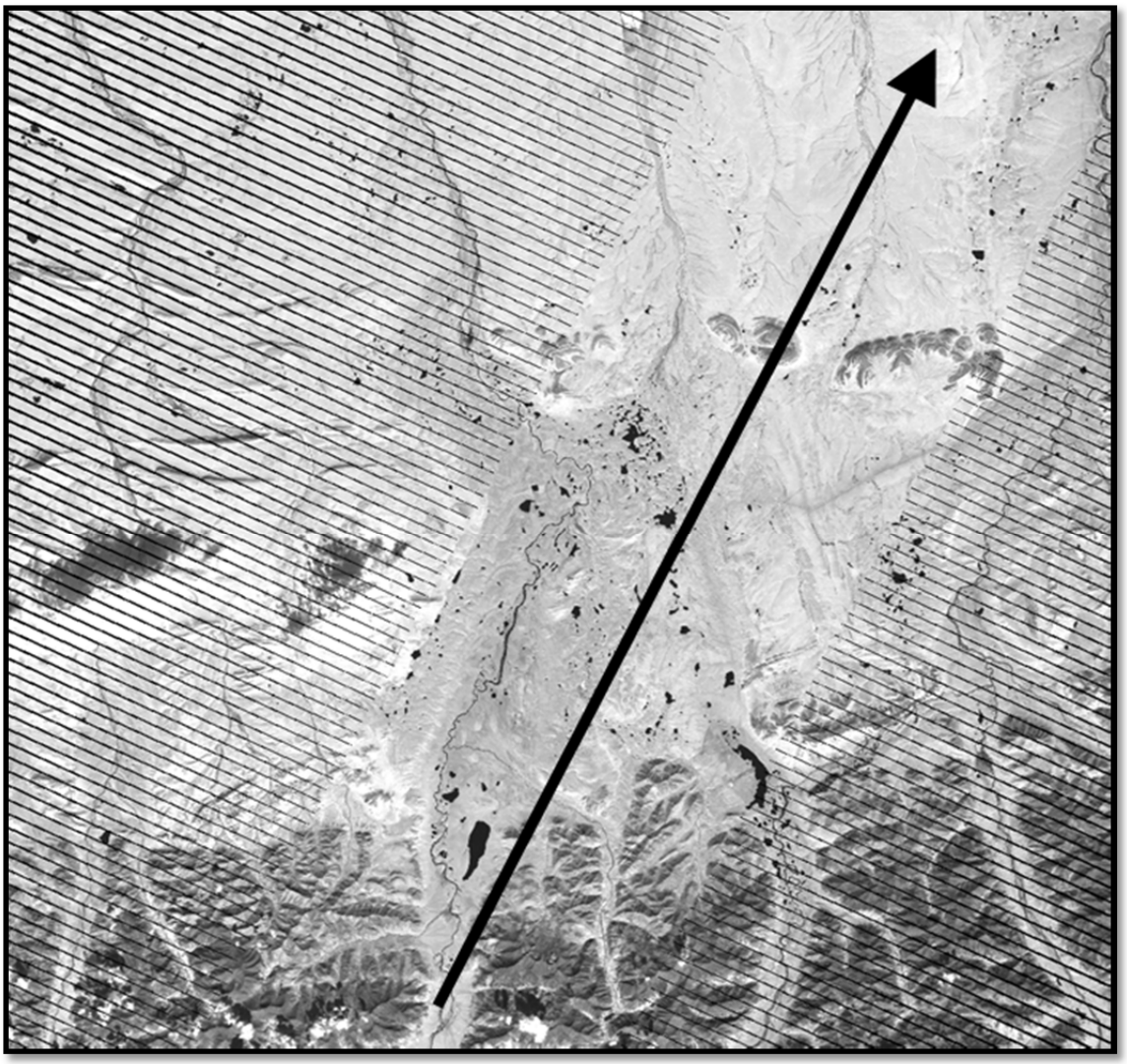

Figure 2.2 2007 Landsat ETM+ Image of the research area. The scan line corrector (SLC) corrected image distortion caused by the curvature of the Earth. The lines represent areas of missing data. NADIR (arrow) was the only area left unaffected.

The SPOT, IKONOS, and AVHRR sensors have been used to derive land cover classifications, monitor vegetation composition and phenology changes, and create hydrologic and digital elevation models within the Arctic (Markon et al., 1994, 1995; Shippert et al., 1995; Hope et al., 1993, 2003, 2005; Jia et al., 2002; and Raynolds et al., 2008; Laidler et al., 2003, 2008; Stine et al., 2010). SPOT 5 High Resolution

Geometrical (HRG) sensor (2002 to present) incorporates a sensor that has 2.5 to 5 meter spatial resolution on its pan band. The multispectral bands are collected at 10 meter spatial resolution. Its spectral coverage, however, is approximately the same as Landsat sensors.

The Earth Observing Satellite (EO-1), launched in 2000, contains the Hyperion and Advanced Land Imager (ALI) sensors. The Hyperion sensor captures 242 bands of information while the ALI sensor captures 10. Both sensors acquire data from basically the same area of the spectrum (visible/near-infrared to shortwave infrared—approximately 400nm to 2500nm). They also have similar spatial resolutions (30m) and are collected in a higher radiometric resolution (16 bits). The higher radiometric resolution increases the sensors' sensitivity to radiation which, in turn, allows them to differentiate between thousands of energy levels. (NASA, 2010)

NASA created the ALI sensor as the next evolution of Landsat type sensors (NASA, 2010). ALI data are expected to span gaps that may exist between the oldest and newest multispectral sensor imagery. All three sensors, TM, ETM+ and ALI, collect EMR data over basically the same spectral range. The continuity of data between the TM, ETM+ and the ALI is considered to be "excellent" (Bryant et al., 2003, p. 1204). However, the Hyperion sensor has been plagued with issues that may be difficult for some researchers to overcome. Issues with sensor calibration are responsible for the redundancy of 24 bands, inaccurate spectral values, and striping (an internal line drop error) that can range from slight to considerable. Data storage requirements, sensor

calibration, and difficulty of use are just three of the problems associated with Hyperion imagery.

While the Hyperion sensor may have its problems, previous studies using Hyperion imagery performed in African agriculture and savannahs (Thenkabail et al., 2004), Canadian rain forests (Goodenough et al, 2003), as well as Asian tropical forests and agriculture (Liew et al., 2002) have shown that the finer spectral resolution (narrow band widths) produced higher classification accuracies than the IKONOS or SPOT 5sensors, which have a much higher spatial resolution. While savannahs, forests and tundra vary greatly, the concept of superseding the high spatial resolution imagery for the higher spectral resolution imagery remains the same.

Detailed technical information, concerning each sensor, can be found at http://landsat.usgs.gov/, http://eo1.usgs.gov/, and http://www.spot.com/, and a concise general description and comparison of the ALI, Hyperion, and ETM+ sensors can be found in Nikolakopoulos, 2007.

2.3 Classification Techniques

2.3.1 Traditional Image Classification Techniques

Traditional classification procedures group pixel values into designated land cover classes or categories through spectral, spatial, or temporal pattern recognition algorithms. Theoretically, individual surface features should have unique spectral signatures that the algorithms group together. However, spectral signatures are often affected by such things as atmospheric composition, slope, aspect, or moisture content

(Carpenter et al., 1997). Historically, spectral pattern recognition is the most commonly utilized classifier that includes the supervised and unsupervised classification techniques (Lillesand et al., 2008).

A supervised classification is driven by a-priori information known by the analyst. These land cover characteristics are incorporated into the clustering algorithm in order to guide the designation of land cover classes. Unsupervised classifications are driven by "natural spectral groupings" (Lillesand et al., 2008:547) of similar pixel values as distinguished by the computer (Jensen, 2004; Lillesand, 2008; Chuvieco and Huete, 2010). Once classification takes place, cell values are changed into numeric labels that identify categories (classes) and no longer represent optical properties (Chuvieco and Huete, 2010) (Figure 2.3).

> Stehman, (2009) states that an accuracy assessment is based on comparing the map depiction of land cover to the true land cover condition. Typically 'ground truth' is not practically attainable, so accuracy assessments evaluate the map land cover relative to some higher quality determination of land cover. These higher quality data, referred to as 'reference data', are used to produce a 'reference land cover classification' that is compared to the 'map land cover classification' (p.5243).

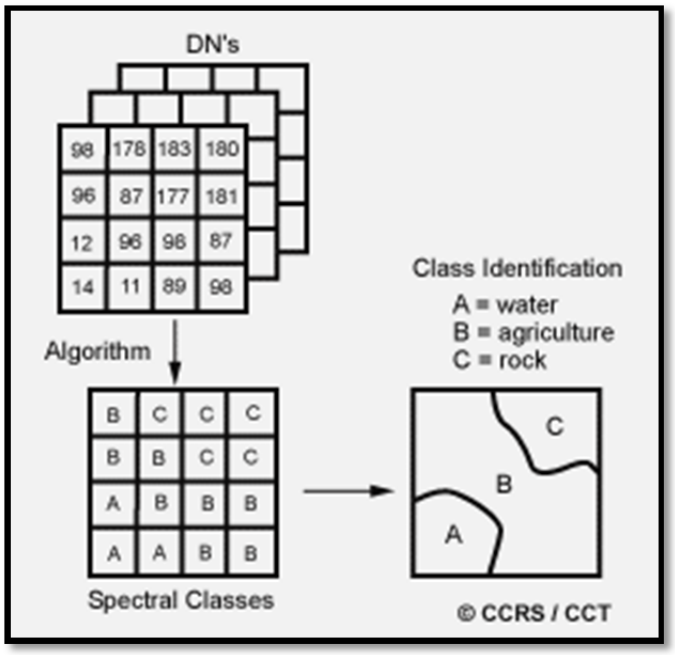

Figure 2.3 Diagram showing how individual pixel values are classified into various classes which represent types of land cover. **http://www.ccrs.nrcan.gc.ca/resource/tutor/fundam/images/unsuper_e.gif**

2.3.2 Non-Traditional Image Classification Techniques

Non-traditional classification techniques allow the analyst to incorporate new types of data, technology, and/or techniques into classification algorithms which can then "streamline or improve the accuracy" (Lillesand, 2008:572) of traditional classification schemas based solely on spectral properties. There are several non-traditional classifiers including fuzzy classification (Oldeland et al., 2010; classification trees (Stine et al., 2010), hybrid classification (Chaudhuri, 2008; Pathak, 2010; Eisner et al., 2005;), Object Oriented (Durieux et al., 2007; Hese et al., 2010; Laliberte et al., 2004), and Artificial Neural Networks (ANN) (Rizvi and Mohan, 2010).

2.4 Utilizing Arctic Land Cover Classifications

All vegetation radiates unique energy information (spectral signatures) that can be recorded by a sensor. Those recordings are transferred into digital format (numbers) that represent the reflective energy values (brightness values BV) of the vegetation. To group land cover into individual categories, or classes, similar BVs are grouped together to represent one class. Like classes can also be combined to represent a defined grouping of vegetation species, such as is the case with this study. The Arctic has intrinsic conditions that often make it difficult for spectral data from the surface to pass through the atmosphere unaltered before reaching the satellite sensor. Various processing techniques and imagery enhancements, such as the Normalized Difference Vegetation Index (NDVI), Seasonally Integrated Normalized Difference Vegetation Index (SINDVI), and Fourier Transform Noise Removal, have been used to aid in land cover analysis (Stine et al., 2010; Hope, 2003; Tucker, 2001; Stow, 2003; Dou, 2002; and Frohn, 2005; Xu and Gong, 2003; and Huete et al., 2003).

Many Arctic studies have relied on land cover classifications derived from satellite imagery. Landsat derived land cover maps have been used to: create time-change analysis (Rees et al., 2003; Tommercik et al., 2003), identify critical habitat (Frohn et al., 2005; Theau et al., 2005; Belchansky et al., 1995; Gratto-Trevor, 1996), create sampling strategies (Shiklomanov and Nelson, 2002), quantify methane emissions (Schneider et al., 2009), identify phenological trends (Olthof and Latifovic, 2007), quantify glacier retreat rates (Bishop et al., 1998; Cullen et al., 2006), and monitor permafrost loss (Hinkel et al., 2007; Tutubalina and Rees, 2001). Walker et al. (1982)

created a classification schema for Alaskan tundra primarily based on dominant species, moisture levels, and its ability to be identified using a Landsat satellite image. Many subsequent Arctic researchers have used this classification schema as the basis of their own, making minor adjustments as required by their research sites' scale, location, or as in this study's case, the additional use of ground cover photographs (Auerbach et al., 1997; Walker and Barry, 1991; Muller et al., 1999; Kutzbach et al, 2004; Stine et al., 2010; and Schneider et al., 2009).

In 1994 Walker et al. published one of the earliest satellite-assisted vegetation maps of the Upper Kuparuk River Basin (UKRB) research area, *Vegetation of the Upper Kuparuk River Region.* The map was created by integrating 1979 through 1982 Landsat Multi Spectral Scanner (MSS) imagery with aerial photography and intense fieldwork. And, while considerable research has continued within the Upper Kuparuk River Basin (UKRB), only two subsequent vegetation maps of this area, at an equivalent scale or higher, have been published (Stine et al., 2010, Patahak, 2010).

Imagery-derived Arctic land cover classifications have been used to identify functional vegetation types (Stow et al., 2007), vegetation greenness trends (Jia, G., 2006), and link large scale (local) biophysical patterns to smaller scale (regional) landscapes (Walker et al., 2002). Kozlenko and Jefferies (2000) used a sequence of SAR images to derive a digital elevation model that, combined with a simulated ice growth curve, produced bathymetric maps of thaw lakes.

Over the past two decades, research in the UKRB has centered on the changing environment attributable to rising temperatures (Bunn et al., 2007; Callaghan et al., 2005;

Epstein et al., 2004). Walker et al. (2006) and Epstein (2004) found evidence to suggest that specie replacements can begin to occur in as little as two growing seasons. Just the increase in deciduous shrubs, such as *Betula nana, Salix pulchra and Salix lantana*, encourages greater species replacement, which, subsequently, promotes warmer temperatures; thus creating a positive feedback cycle that ensures shrub expansion and increasing temperatures (Grosse et al., 2006; Liston et al., 2002; Sturm et al., 2001, 2005, 2006; Tape et al., 2006; Walker et al., 2002; Reidel et al., 2005; Beck et al., 2005, Myers-Smith, 2007; Pomeroy et al., 2006). Epstein et al., 2004 identified "shrubs and mosses" as "key indicators of [specie] community change" (p. 1325).

CHAPTER III

MATERIALS AND METHODOLOGY

3.1 Data

The imagery selected for this research was driven by the availability of quality imagery with an acquisition date that corresponded to within a couple of years of the fieldwork performed during the summers of 2006 to 2008. There was only 1 cloud free, summer image for both the Hyperion and ALI sensors; August 17, 2004.

Each sensor collects a specific number of image bands corresponding to specific wavelengths of the electromagnetic radiation (EMR) spectrum (Appendix A). Datasets for Alaska were obtained from the USGS image warehouse at the University of Maryland's *Global Land Cover Facility* (www.land cover.org), the USGS EROS data center (http://glovis.usgs.gov), SPOT Inc., and the University of Alaska, Fairbanks. Both the Hyperion and ETM+ sensors are experiencing failures, rendering individual bands, or sections, of an image unusable. Of the original 242 Hyperion bands, only a total of 82 were used in the analysis (20 – 53, 85 – 96, 102 – 118, and 137 – 155) because the signal to noise ratio of many of the mid to far SWIR bands was extremely low and could not be satisfactorily corrected. In 2003, the ETM+ sensor's scan line corrector (SLC) failed causing the outer extents of its imagery to contain areas where data was not collected, resulting in multiple black stripes (Figure 2.2). Damaged or corrupt data layers are caused by failures of the system, the sensor, or its programming (ERDAS, 2010).

3.2 Study Area Description

The research area (Figure 3.1) is located within the Upper Kuparuk River Basin (UKRB), which is located on the North Slope of Alaska. The research area is approximately 93.24 km^2 (36 mi^2). The western extent of the research area is limited by the ALI image, while the eastern is restricted by the width of the Hyperion image. Toolik Lake (68.63^{o}N/ 149.6^o W) resides approximately at the center of the research area. Glacial landforms prevalent within this region include moraines, erratics, askers, and kettle lakes (Hamilton, 2002). Vegetation classifications derived from remotely sensed data within this region are primarily vegetation assemblages, i.e. groups of species (Stine et al., 2010; Hope, 2003; Tucker, 2001; Walker et al., 1999; Stow, 2003; Dou, 2002; and Frohn, 2005; Xu and Gong, 2003; and Huete et al., 2003).

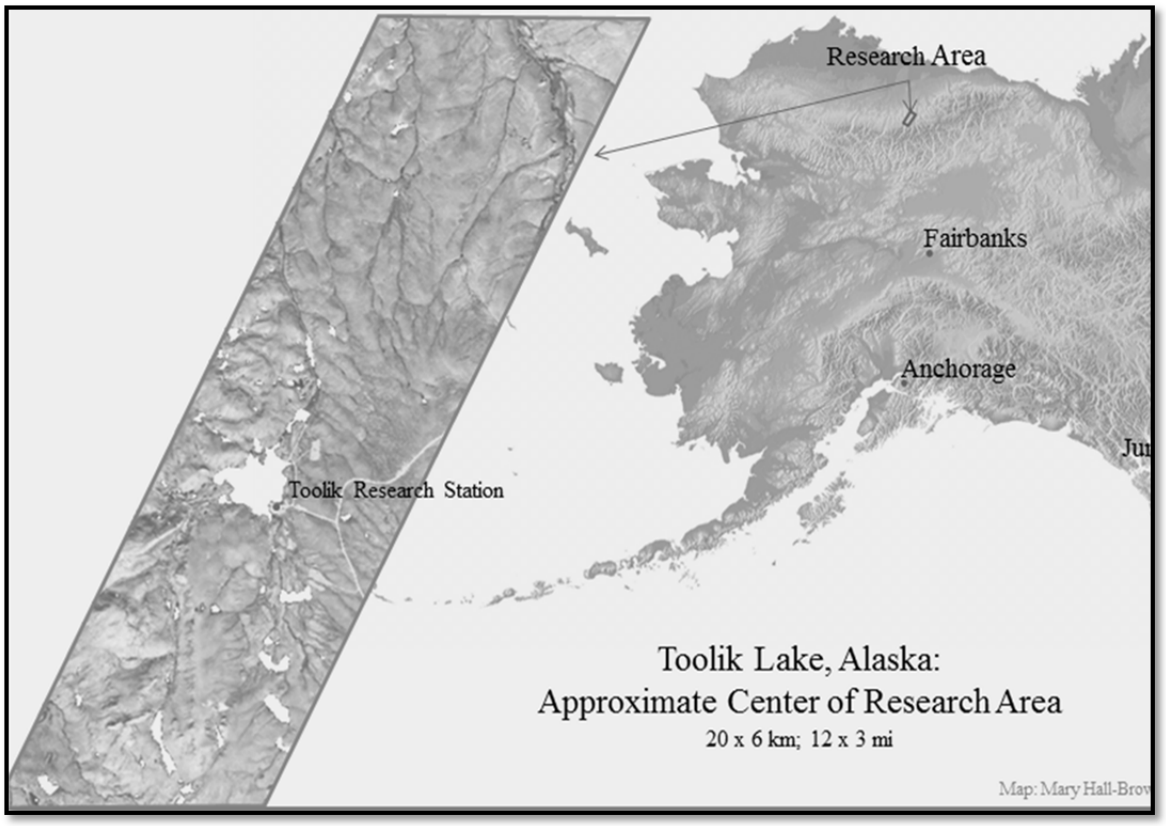

Figure 3.1 Research Area

3.3 Image Processing

Irregularities in BVs within an image can be caused by many issues, although, they are most commonly caused from atmospheric and/or topographic effects plus the "differing sensitivities or malfunctioning of the [sensor's] detectors" (ERDAS, 2005, p. 159). Software programs used in this research to perform all processing include: ArcGIS 10[3], ERDAS Imagine[4] 2010, Pathfinder Office 3.1[5], SAS 9.2 Silver Edition, Microsoft Office

[3]Environmental Research Systems Institute. 2012
[4] Intergraph Corporation. 2012.
[5] Trimble Navigation Limited, 2012

Suite, 2010[6].

3.3.1 Geometric Correction

Geometric correction was performed to align the images to their on-Earth location. Approximately 200 ground control points (GCPs) were collected using the Trimble XH Pro and the Garmin XP2 receivers. Large landscape features were used as the basis to select an additional 700 to 800 points within the Hyperion and ALI images in order to rectify each to the 2005 SPOT 5 image (Bruzzone and Persello, 2008). A degraded 30m SPOT 5 image was created to assist with the georectification process. Resolution degradation is a process that generalizes the attributes of neighboring pixels into a single larger pixel which retains less detail, but is still representative of the group. For example, 36 pixels of the SPOT 5 image (5m) made one 30m pixel. The projection used for all imagery was the Universal Transverse Mercator (UTM) coordinate system, Zone 6, with the World Geodetic System as the datum (WGS 84). The root mean squares (RMS) error for each image was less than one pixel (30m).

The RMS error is calculated by

$$\text{RMSE} = \frac{\sqrt{(X_i - X_j)^2 + (Y_i - Y_j)^2}}{\text{Total number of points}}$$

where *i* is the position of the point on the image and *j* is the position of the point on the ground. X and Y are easting and northing positions (Jensen, 2005).

[6] Microsoft Corporation, 2012

3.3.2 Radiometric Correction

Radiometric resolution defines a sensors "ability to discriminate very slight differences in energy" (CCRS, 2008, p. 1.). The possibility of obtaining greater levels of detail is determined by the radiometric resolution of a sensor [i.e. 8 and 16 bits]. The higher quantization number equates to higher levels of detail being recorded. The 16 bit resolution is 256 times greater than that of an 8 bit sensor. The Hyperion and ALI sensors store data at 16 bit radiometric resolution while the SPOT and ETM+ sensors store data in an 8 bit data format. Processing techniques for radiometric correction address "variations in the pixel intensities (BV) that are not caused by the object or scene being scanned" (ERDAS, 2006, p. 159). The Hyperion sensor has uncalibrated, overlapping, and misaligned sensor arrays that resulting in no data, striping or noise, rendering some bands unusable (Thenkabail, 2004; Goodenough et al., 2003).

The Principle Component Analysis is a technique employed to mitigate or minimize image noise and striping. "The central idea of principal component analysis (PCA) is to reduce the dimensionality of a data set consisting of a large number of interrelated variables, while retaining as much as possible of the variation present in the data set" (Jolliffe, 2002, p. 1; ERDAS, 2010). The PCA procedure produced uncorrelated variables (components) which were ordered so that the first component contains the highest variance from the original data (Jensen, 2005). For example, the first component provided the majority of variability within the image, while all subsequent layers included lowering levels of variation. Four PCA analyses were performed using Hyperion bands: 85 to 96, 102 to 115, 137 to 145, and 146 to155. In all PCAs, the first

component incorporated over 93% of the variability within the group (Figure 3.2). PCAs were also created to explore the bands selected from the SDA along with a combination of VNIR bands 20 through 53, which is shown in Figure 3.3.

146-148_151-155.img

Eigen Matrix:	Component *p*							
	1	2	3	4	5	6	7	8
bnd1	0.32389	-0.0576	-0.1257	-0.1327	-0.7679	0.14964	0.49484	0.0377
bnd2	0.35629	0.31798	0.45029	-0.1999	0.16661	-0.1079	0.10292	0.69226
bnd3	0.3581	0.22702	0.42951	-0.3693	0.03017	-0.1246	-0.0607	-0.6923
bnd4	0.37291	-0.4854	-0.2395	-0.0557	0.50998	-0.2409	0.49275	-0.0628
bnd5	0.37359	-0.2366	-0.3384	-0.4646	0.02788	0.37189	-0.5623	0.13715
bnd6	0.36726	0.41381	-0.1473	0.48684	0.25027	0.58352	0.12281	-0.1303
bnd7	0.34144	-0.5097	0.43673	0.5458	-0.1915	-0.0476	-0.3095	0.01664
bnd8	0.3314	0.3485	-0.4611	0.22831	-0.1466	-0.6414	-0.2665	0.01023

	Eigen-values: bands	**percent variability**
bnd1	0.00773	**93.9**
bnd2	0.00011	1.34
bnd3	0.00009	1.09
bnd4	0.000078	0.95
bnd5	0.000065	0.79
bnd6	0.000063	0.77
bnd7	0.0000545	0.66
bnd8	0.000041	0.5
	0.0082315	

Figure 3.2 The first component of a PCA created from bands 146, 147, 148, 151, 152, 153, 154, and 155 incorporated almost 94% of all the pixel variability in all 8 bands.

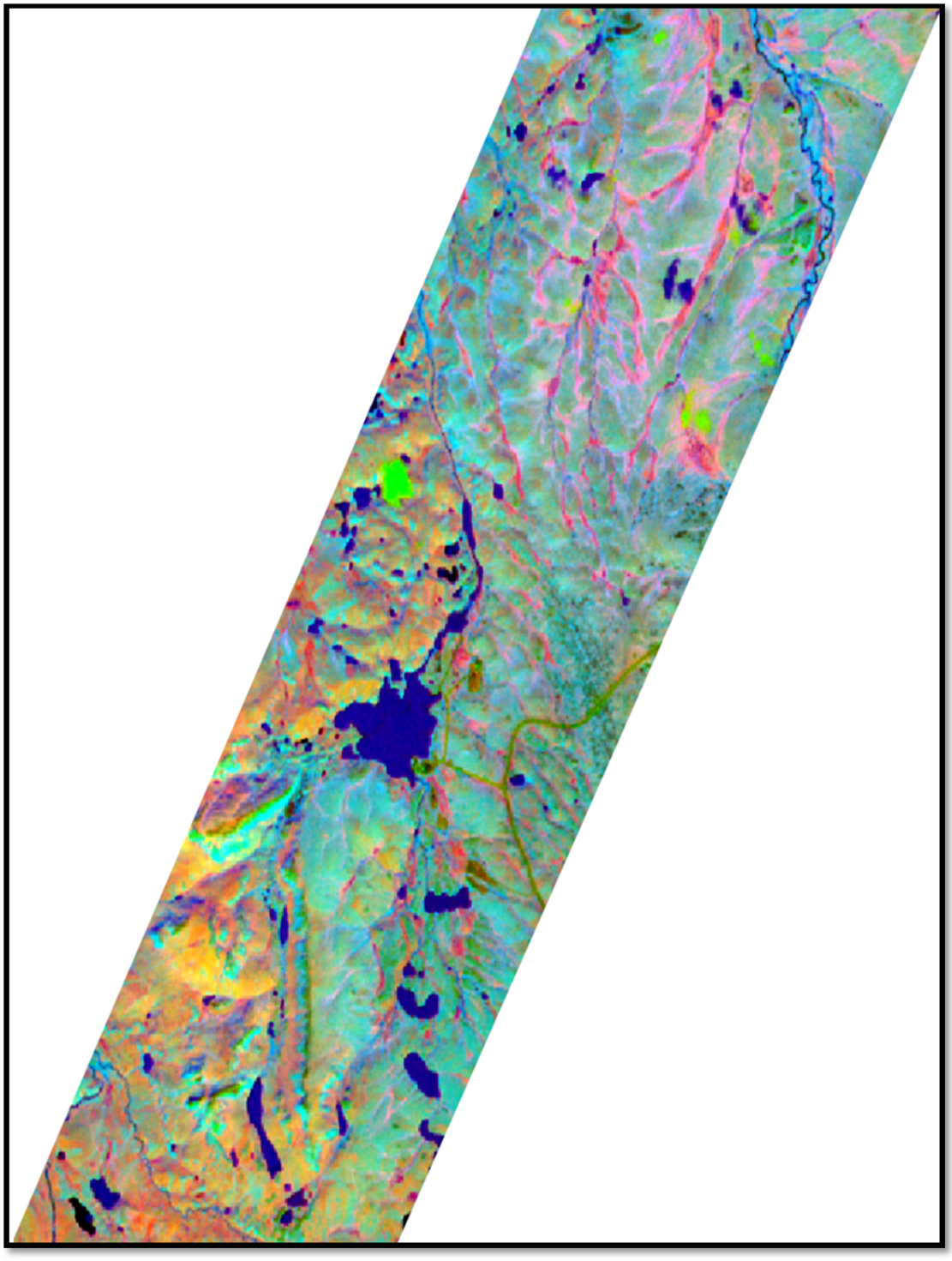

Figure 3.3 A PCA containing five components was created using Hyperion bands 20 – 53. The first two components contained 99% of all variability in the bands. Components 5, 4, and 2 (RGB) are displayed.

3.3.3 Buffering and Masking

The Dalton Highway (Haul Road) connects Fairbanks, Alaska to the oil fields of Prudhoe Bay. It is constructed and maintained with gravels, sands, clays and silts which, when disturbed, produce dust that scatters across the surrounding landside. Arctic researchers have shown that this fine dust affects BVs of the surrounding vegetation (Walker and Walker, 1991; Auerbach et al., 1997). Buffering and masking and is a two-step process where BVs are replaced with zeros, thereby excluding them from the classification process (ERDAS, 2010). Following Walker and Walker (1991), distances of 300 and 90 meters were designated as the buffer distance for the Dalton Highway and Toolik Field Station. A mask containing the buffered area was used to replace pixel values with zeros (Figure 3.4).

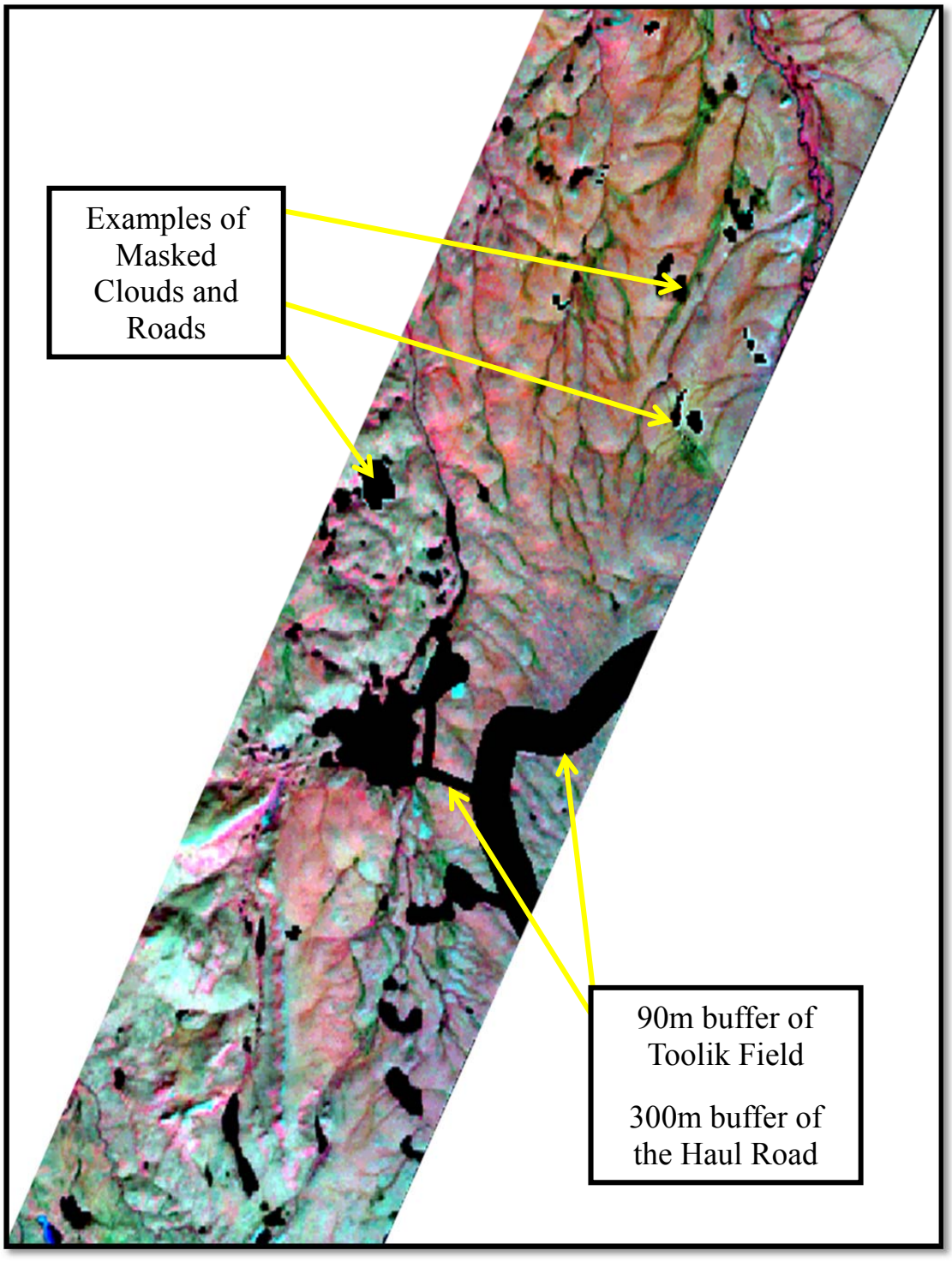

Figure 3.4 Hyperion image showing where masks and buffer are located.

3.3.4 Conversion to Surface Reflectance

The conversion of at-sensor BVs to surface reflectance values were performed before classification analysis (Thenkabail et al., 2004; Goodenough et al., 2003). At-sensor radiance is converted to spectral radiance, then planetary reflectance and finally surface reflectance (Figure 3.5). The final adjustment is for atmospheric conditions such as water vapor or other aerosols.

Hyperion BVs are converted to spectral radiance values using scaling factors of 40 for the visible and VNIR bands, and 80 for SWIR bands. BVs for ALI imagery are scaled by a factor of 300. The ETM+ and SPOT 5values are converted to radiance within a formula that uses the sensors gain and offset. The gain and offset values are given in the sensor's documentation. Hence spectral radiance values are:

Hyperion VNIR bands = BV/40 (1)

Hyperion SWIR bands = BV/80. (2)

ALI = BV/300. (3)

TM and ETM+ = BV x Gain + Offset (4)

SPOT = (BV/Gain) + Offset (5)

Spectral radiance is further converted to planetary reflectance (apparent reflectance) with the following formula:

$$\rho_P = \frac{\pi L_\lambda d^2}{ESUN_\lambda \cos\theta_s} \quad (6)$$

Where ρ_p is the at-satellite exo-atmospheric reflectance, L_λ is the radiance, *d* is the earth to sun distance in astronomic units on the acquisition date. $ESUN_\lambda$ is the mean solar exo-atmospheric irradiance or solar flux, and θ_s is the solar zenith angle in degrees (Markhan and Barker 1987; Neckel and Labs, 1984; Thenkabail et al., 2003).

This study used the improved dark object subtraction (DOS) technique to achieve surface reflectance (Chavez, 1986 and 1996). This method of atmospheric correction uses BV's derived directly from the image. Since ancillary data are not required, this method becomes very beneficial when historical atmospheric data cannot be obtained (Clark et al., 2010). The DOS methodology basically resets the histogram value of the darkest feature in the image to zero.

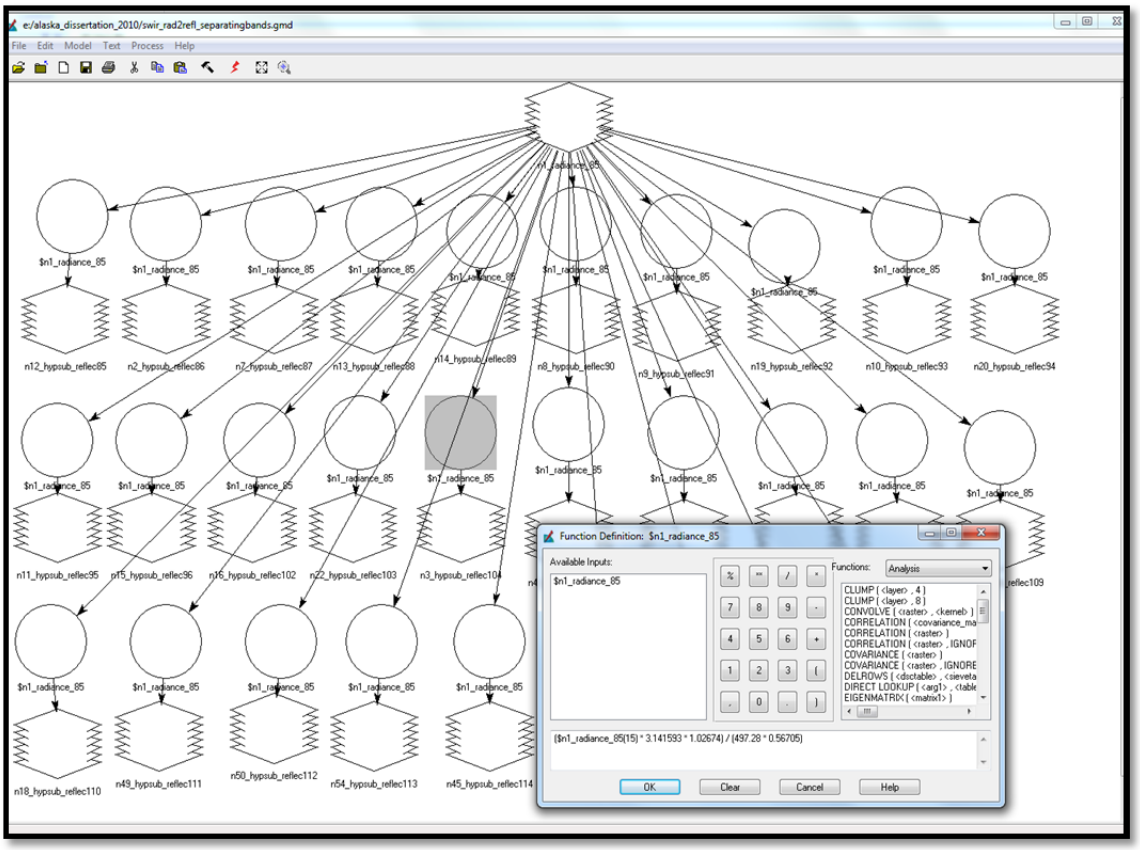

Figure 3.5 Function dialog box displays the formula to convert at-sensor radiance values to surface reflection values and how it was applied to individual Hyperion bands.

3.4 Data Analysis

Statistical Analyses such as correlation and stepwise discriminant analyses (SDA) were performed on the Hyperion data to eliminate redundant band information while identifying optimum bands to include within the classification analysis. A total of 82 bands were used in this study (Table 3.2).

3.4.1 Stepwise Discriminant Analysis (SDA)

The SDA process, as described by Murphy et al. (2008, p. 6) states that:

> This discriminant analysis method uses a stepwise variable selection procedure to find a subset of variables that gives good classification results. Each stage of the algorithm involves two steps:
> - Determine if a variable (not already selected) would contribute to the discriminant analysis model. If the variable improves the model, it is added to the model
> - Determine if any selected variables should be removed from the discriminant analysis model. If a selected variable does not contribute to the model, then it is removed (p.6).

Basically, the SDA statistical method reduces the dimensionality of the image data by identifying specific bands that best represent land cover classes, thereby theoretically producing higher classification accuracies (Thenkabail et al., 2004; Serpico, and Moser, 2006). Since much of the research area was not represented by ground truth points (GTPs), an initial procedure was performed to extrapolate the groundcover found at the GTPs to the entire research extent.

An unsupervised classification consisting of 100 categories was performed on a Hyperion image created from bands 20 through 53 and an ALI image containing bands 3 through 10. GTP's were used to only classify categories that corresponded to them. This was used to create a thematic map of known and unknown land cover areas, which, was used as a mask to remove the unknown land cover areas from the Hyperion and ALI images. The image of known land cover was then used to create 500 random points. Points that fell outside the known parameters of the map were deleted. A total of 399 points corresponded to pixels of known vegetation types in the image. In ArcMap, BVs

of these pixels were extracted from the Hyperion data bands in order to create a data set that could be utilized within SAS. In an effort to incorporate as many Hyperion bands as possible, both individual bands and several PCAs of slightly striped bands from 85 through 163 were created and used within the SDA. The process is shown in Figure 3.6. The Stepwise Discriminant Analysis was performed using this final dataset (Figure 3.7). The 2005 SPOT 5 image, 2007 aerial imagery (1ft resolution), and photographs taken from helicopter flights were used for additional confirmation of classification accuracy.

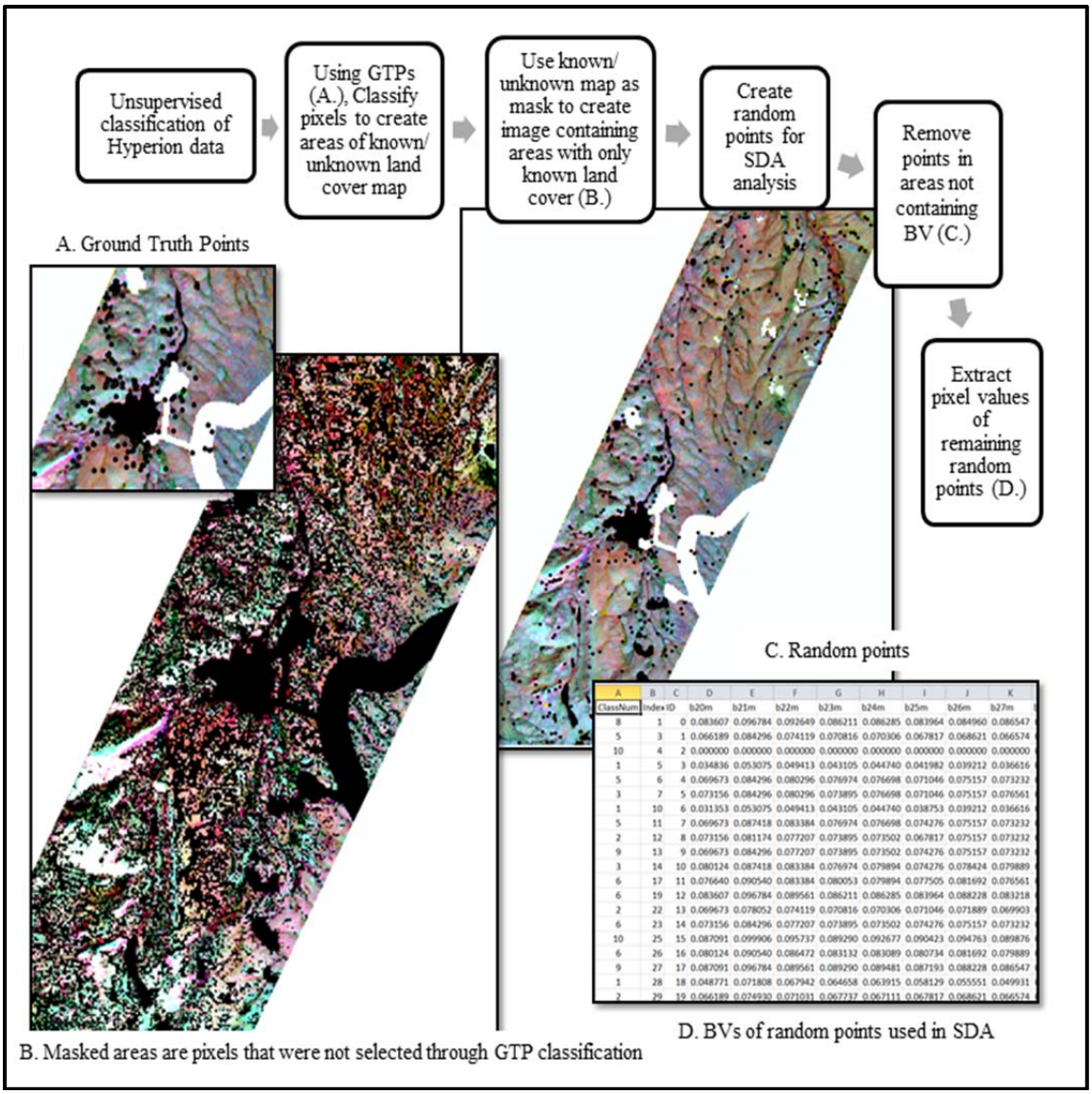

Figure 3.6 Steps to obtaining pixel values for use in Stepwise Discriminant Analysis.

```
PROC STEPDISC data=work.B20_pca155 SLENTRY=0.05 SLSTAY=0.05;
Class Classnum;
VAR b20m b21m b22m b23m b24m b25m b26m b27m b28m b29m b30m b31m b32m b33m b34m b35m
    b36m b37m b38m b39m b40m b41m b42m b43m b44m b45m b47m b48m b49m b50m b51m b52m
    b53m pca85_96 pca102_115 pca116_118 pca137_145 pca146_155;
Quit;
```

Figure 3.7 Stepwise Discriminant procedure statement used in SAS.

3.5 Ground Truth Data Collection

Approximately 200 GTPs were collected during the summers of 2006 through 2008. For points that fell in visited watersheds, the stratified random sampling method was utilized to generate points. Other GTPs were collected when the opportunity and/or ease of collection was present (e.g. near Toolik Field Station or near Highway 11). GTPs are collected using the Trimble XH Pro and the Garmin XP2 receivers.

3.6 Classification Process

The land cover classification schema utilized in this research is based on the classes produced by Walker et al., 1994, through his fieldwork and the use of Landsat imagery. The classification scheme used in this study incorporates slight changes from Walker's as was determined by Drs. Peter Ray and Roy Stine through field inspection and photography. The nine classes utilized within this research reflect the scope and resolution of the study are presented in Table 2 (Stine et al., 2010; Ray, 2006; Chaudhri, 2008; Pathak, 2010). Examples of classes are shown in Figure 3.8.

The Iterative Self-Organizing Data Analysis Technique (ISODATA) is a computer driven classification process that groups like spectral signatures within an unsupervised classification. The ISODATA process runs iterative scans clustering and reclustering the spectral data into the desired number of classes (Jensen, 2005). For this study, 100 initial clusters were created, which, after identification, were merged into the final ten classes. Spectral signatures for each class within the Hyperion and the ALI images are shown in Figures 3.9 and 3.10. While there are similarities in the two sensors' signatures, the narrow bandwidth of the Hyperion sensor (10nm) makes its signatures more distinctive to the vegetation species rather than the assemblage.

Table 2. Vegetation Community Classifications and Species Composition.
(Pathak, 2010, modified)

Class	Description
Water	Lakes, streams, and rivers
Wet Graminoid Tundra complex	*Carex aquatilis*, *Carex chordorrhiza, Eriophorum scheuchzeri* (growing in shallow water regions)
Barrens	Barren surfaces, sparsely vegetated, rocks covered with lichens
Heath complex	*Festuca altaica, Empetrum hermaphroditum, Loiseleuria procumbens, Dryas octopetala,* along with *Cassiope tetragona, Salix phlebophylla*
Shrubs complex	*Betula spp., Salix spp., Sphagnum spp.*
Moist Acidic Tussock tundra complex (MAT)	*Eriophorum vaginatum, Carex bigeloii, Betula nana, Salix pulchra, Sphagnum spp.*
Moist Non-Acidic Tussock tundra complex (MNT)	*Saliz reticulate, Saxifraga oppositifoli, Carex bigelowii, Carex membranacea, Dryas integrifolia, Ledum decumbens, Equisetum arvens*
Fen complex	*Carex rariflora, Carex rotundata,* and mosses like *Sphagnum spp., Carex chordorrhiza, Carex aquatilis* and mosses like *Tomentypnum nitens*
Mountain Meadow complex	*Carex bigelowii, Cassiope tetragona, Saliz chamissonis*

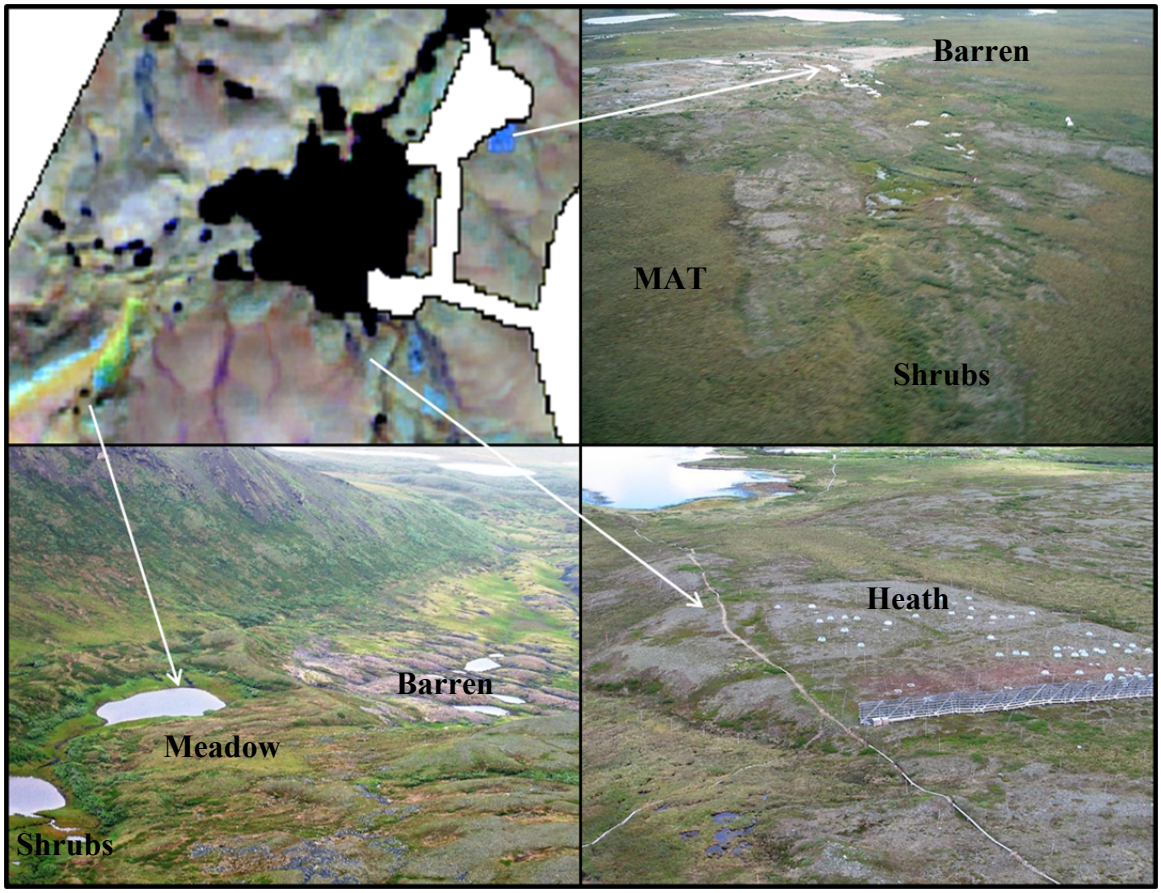

Figure 3.8 Examples of land cover identification derived from ancillary data.

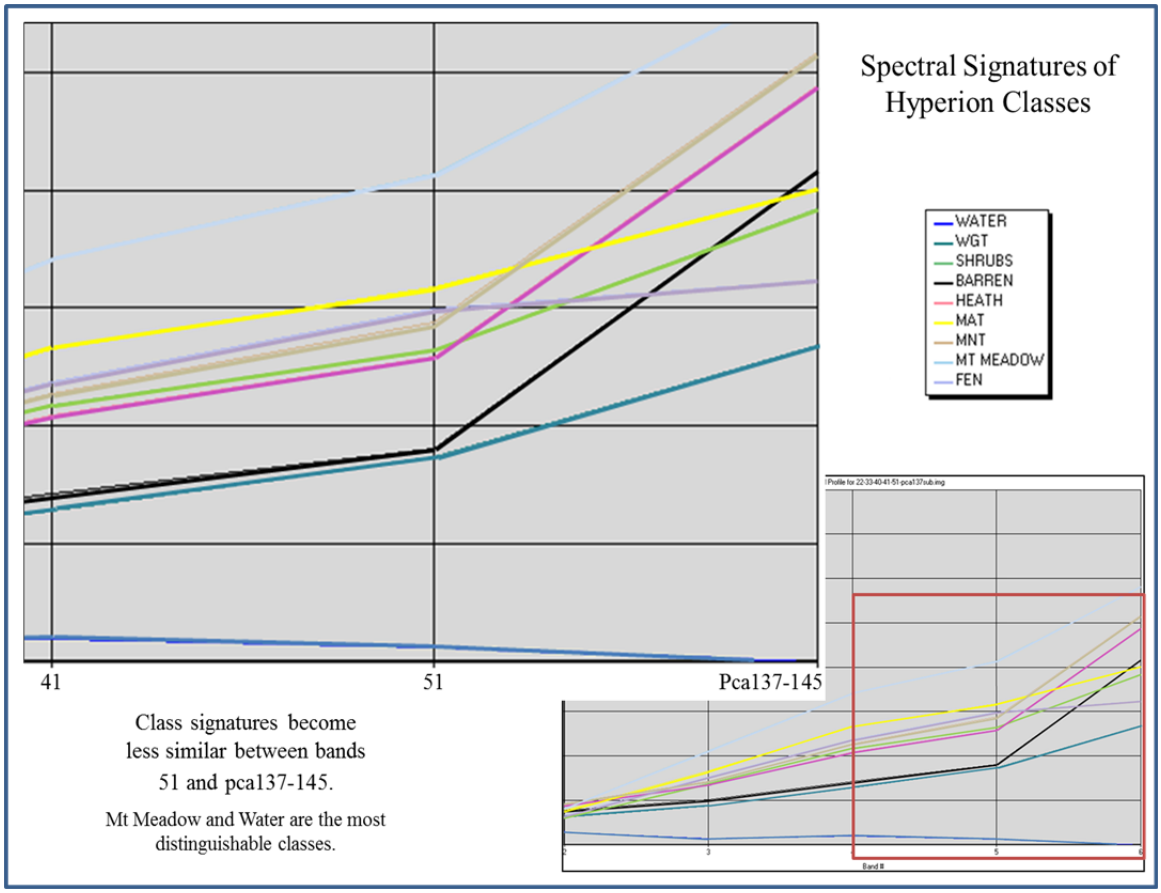

Figure 3.9 Spectral signatures for vegetation of selected Hyperion bands.

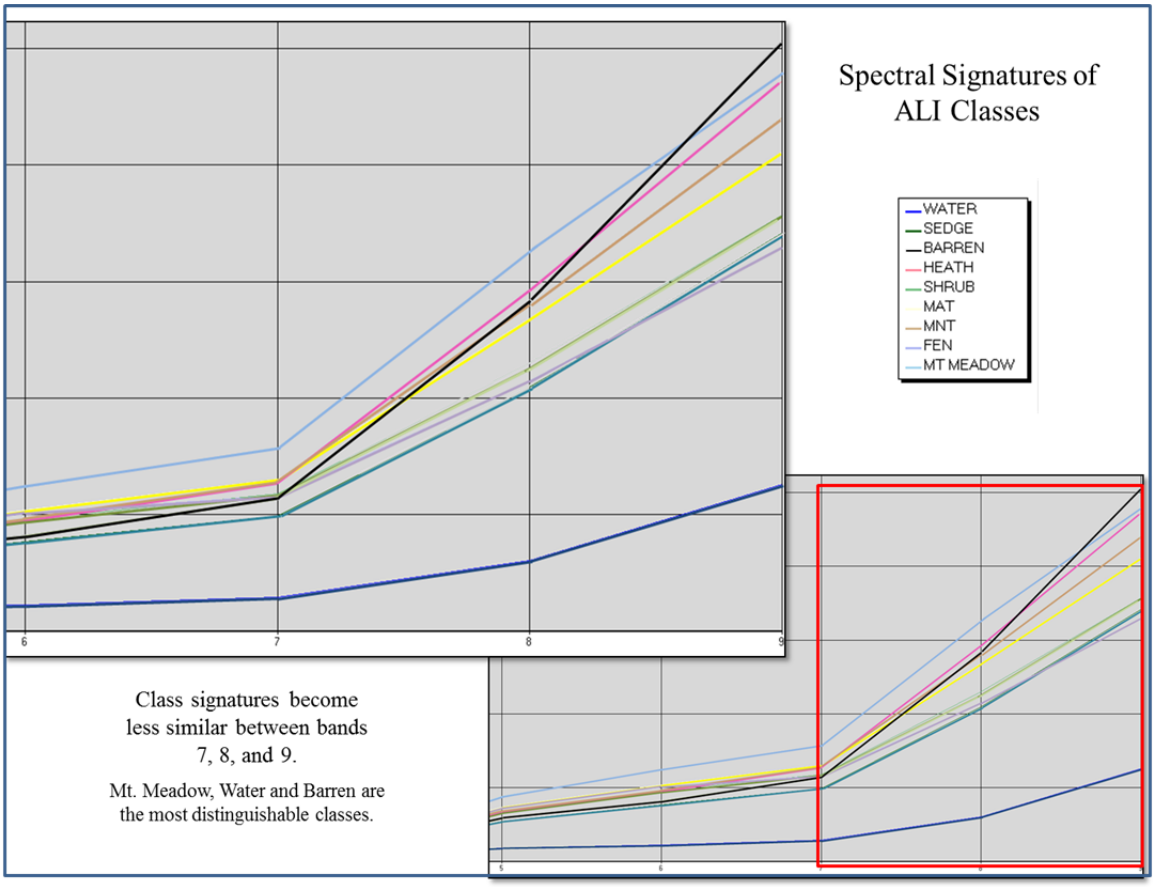

Figure 3.10 Spectral signatures for vegetation of ALI bands.

3.7 Accuracy Analysis

Accuracy assessments were performed using the Stratified Random Sampling Method (SRSM). An advantage of using the SRSM is the unbiased sample selection it produces (Stehman, 1997). The SRSM is a sampling scheme that incorporates the proportionally correct number of samples for each class in the analysis. However, with small classes (e.g. Fen and Mt Meadow) it is often difficult finding enough sampling sites for an exact proportional sample. An error matrix was created by the comparison of the referenced to classified map thus "describ[ing] classification accuracy and

characteriz[ing] errors" (Jensen, 2005, p.499). Two such errors are the Producers and Users error, are also known as the errors of omission (omitted from the correct category) and commission (included with the wrong category). Four standard statistical tests were used to measure the accuracy of the land cover classification (Figure 3.11). They include the overall accuracy (7), the Kappa statistic (8), and the Users and Producers accuracy (9 and 10) where *P* is the proportion of area, *i* (row) is the classified land-cover class, and *j* (column) is the reference land-cover class (Okeke and Karnieli, 2006; Congalton and Green, 2009; Jensen, 2004; Gorham, 1991; Kuzera and Pontius, 2008; and Stehman, 1997).

The overall accuracy reports the "agreement or accuracy between the remote-sensing derived classification map and the reference data" (Jesnen, 2005, p. 507). The conditional kappa statistics is a "coefficient of agreement" that the row and column classifications are the actual categories of land cover *i* and *j* (Czaplewski, 1994; Foody, 1992). 300 stratified random points were generated for the accuracy analysis and are used to create the final reference map. As the reference map is created from a procedure where the land cover classes of surrounding pixels (3 X 3 moving window) are taken into consideration when defining the land cover of a central pixel (focal analysis) many original pixel values were altered (Figure 3.12). Other possible sources of error resulting in misclassification are: the transitional areas between neighboring classes (such as can be caused by elevation changes or proximity to water tracks), shadowed pixels, warping caused from 2nd or 3rd order polynomial transformations performed during the rectification process, and the reclassification of pixels during the accuracy assessment

(Walker et al., 2001; Munger, 2007; Stine et al., 2010; Chaudhri, 2008; Goodenough et al., 2003).

Overall accuracy, $$P = \sum_{k=1}^{n-1} P_{kk} \quad (7)$$

Kappa, $$K = \frac{P - \sum_{k=1}^{n-1} P_k + P + k}{1 - \sum_{k=1}^{n-1} P_k + P + k} \quad (8)$$

Users accuracy, $$P_i = \frac{P_{ii}}{P_{i+}} \quad (9)$$

Producer's accuracy, $$P_j = \frac{P_{jj}}{P_{j+}} \quad (10)$$

Figure 3.11 Standard tests used in accuracy analysis.

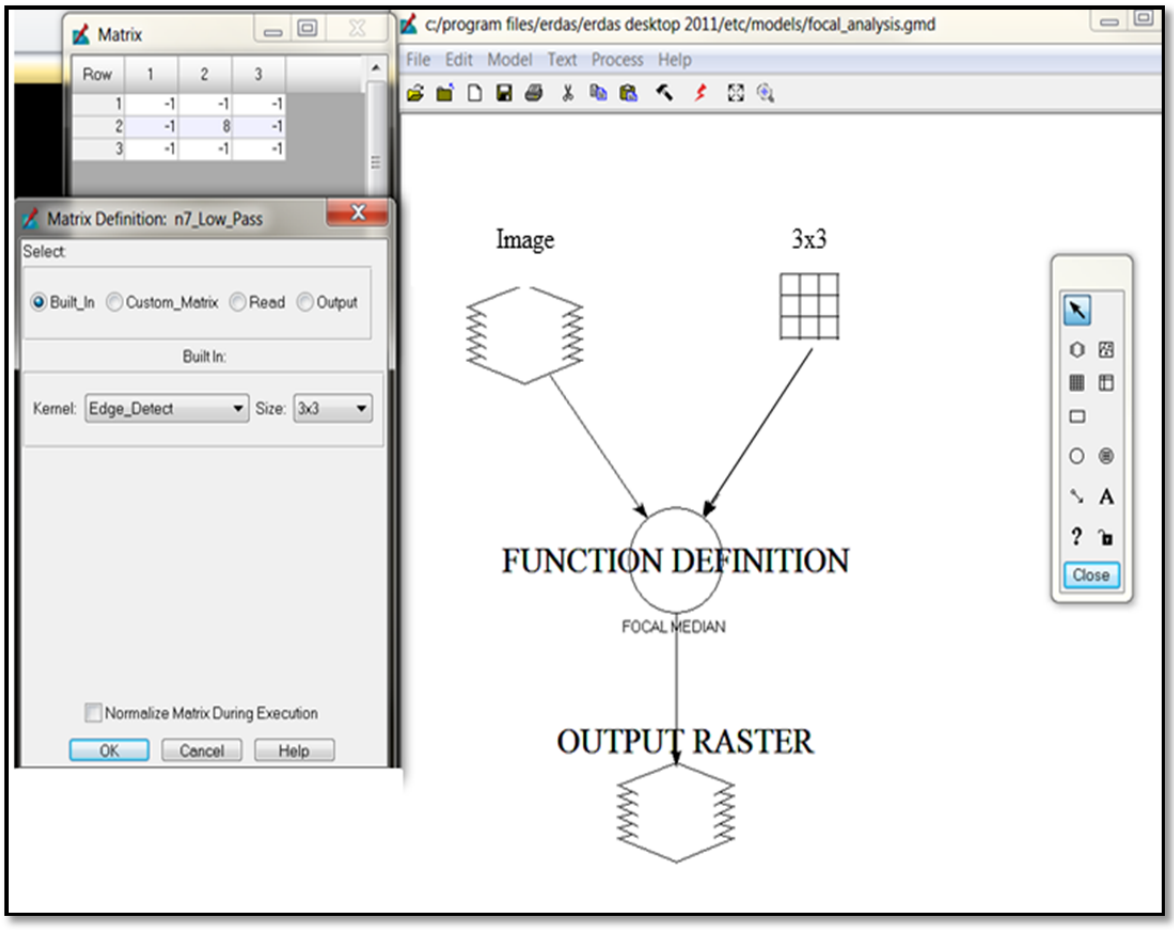

Figure 3.12 Focal analysis process as performed within an accuracy assessment. A moving 3X3 window generalizes adjacent pixel values.

CHAPTER IV

RESULTS AND DISCUSSION

The focus of this research is to determine whether the use of free Hyperion and ALI satellite imagery can identify specific Arctic vegetation assemblages well enough to produce classification accuracies that compare to, or are an improvement over, the classification accuracies derived from very expensive high spatial resolution imagery.

4.1 Selected Bands

4.1.1 Hyperion

From the original bands entered into the SDA, 20 meet the significance level (0.05) for inclusion into the model. The first 6 (51, 33, 22, pca137-145, 40, and 41 in order of selection) have a Wilk's Lambda of at least 0.01 and are incorporated into the final image (Figure 4.1 a and b). Band 22 (avg. λ 569.27nm) lies in the green region, band 33 (avg. λ 681.20nm) the red region, bands 40, 41, 51 and pca137-145 (average λs 752.43nm, 762.60nm, 864.35nm, 1517.83nm, and 1598.51nm) lie in the NIR to MIR region of the EMR spectrum.

Stepwise Discriminant Analysis			
Observations	399	Variable(s) in the Analysis	38
Class Levels	10	Variable(s) will be included	0
		Significance Level to Enter	0.05
		Significance Level to Stay	0.05

Class Level Information			
ClassNum	Frequency	Weight	Proportion
1	36	36	0.090226
2	42	42	0.105263
3	42	42	0.105263
4	56	56	0.140351
5	39	39	0.097744
6	50	50	0.125313
7	38	38	0.095238
8	24	24	0.060151
9	42	42	0.105263
10	30	30	0.075188

a.

Stepwise Selection Summary								
Step	Entered	R-Sqr	FValue	Pr > F	Wilk's Lambda	Lambda	Corrltn	ASCC
1	b51m	0.8787	313.24	<.0001	0.1212	<.0001	0.0976	<.0001
2	b33m	0.6288	73.04	<.0001	0.0450	<.0001	0.1673	<.0001
3	b22m	0.3927	27.81	<.0001	0.0273	<.0001	0.2055	<.0001
4	pca137_145	0.2887	17.41	<.0001	0.0194	<.0001	0.2272	<.0001
5	b40m	0.261	15.11	<.0001	0.0143	<.0001	0.2528	<.0001
6	b41m	0.2182	11.91	<.0001	0.0112	<.0001	0.2703	<.0001

b.

Figure 4.1 a. Classifications showing number of points within class and their proportions.
b. The Wilk's Lambda of selected Hyperion bands.

4.1.2 ALI

Within the ALI's set of bands, the first band is a panchromatic image having a spatial resolution of 10m. As all other bands have a spatial resolution of 30 meters (2 through 10) band 1 is not included within the SDA analysis. From the nine bands entered into the SDA, all nine meet the significance level (0.05) to stay in the model. However, as with the Hyperion SDA, a Wilk's Lambda of at least 0.01 is utilized as the minimum value for a band's inclusion into the final ALI image. The final selection is SDA bands 6, 9, and 5 which lie in the NIR and MIR region of the EMR spectrum (Figure 4.2 a and b).

The Method for Selecting Variables is STEPWISE			
Total Sample Size	399	Variable(s) in the Analysis	9
Class Levels	10	Variable(s) Will Be Included	0
		Significance Level to Enter	0.05
		Significance Level to Stay	0.05

Number of Observations Read	399
Number of Observations Used	399

Class Level Information				
ClassNum	Variable Name	Frequency	Weight	Proportion
1	1	36	36.0000	0.090226
2	2	42	42.0000	0.105263
3	3	42	42.0000	0.105263
4	4	56	56.0000	0.140351
5	5	39	39.0000	0.097744
6	6	50	50.0000	0.125313
7	7	38	38.0000	0.095238
8	8	24	24.0000	0.060150
9	9	42	42.0000	0.105263
10	10	30	30.0000	0.075188

a.

Stepwise Selection Summary									
Step	Number In	Entered	Partial R-Square	F Value	Pr > F	Wilks' Lambda	Pr < Lambda	Average Squared Canonical Correlation	Pr > ASCC
1	1	b6	0.8949	368.02	<.0001	0.10510071	<.0001	0.09943325	<.0001
2	2	b9	0.7221	112.01	<.0001	0.02921012	<.0001	0.17949460	<.0001
3	3	b5	0.5107	44.89	<.0001	0.01429160	<.0001	0.23459635	<.0001
4	4	b8	0.4865	40.63	<.0001	0.00733887	<.0001	0.28797005	<.0001
5	5	b7	0.2301	12.78	<.0001	0.00565042	<.0001	0.30755995	<.0001
6	6	b1	0.1662	8.50	<.0001	0.00471130	<.0001	0.31478969	<.0001
7	7	b4	0.1985	10.54	<.0001	0.00377616	<.0001	0.32816995	<.0001
8	8	b3	0.2590	14.84	<.0001	0.00279798	<.0001	0.34703681	<.0001
9	9	b2	0.1688	8.60	<.0001	0.00232563	<.0001	0.35924503	<.0001

b.

Figure 4.2 a. Classifications showing number of points within class and their proportions.
b. The Wilk's Lambda of selected ALI bands.

4.2 Accuracy Analysis and Classification Results

4.2.1 Hyperion

While vegetation classes appear to be easily discernible (Figure 4.3) on the Hyperion image, the similar spectral signatures actually make it difficult to create spectrally distinct end members for each class. Classes like MAT, MNT, and Shrubs that share vegetative species confuse spectral distinction even further. (MAT, MNT, and Shrubs all contain the dwarf shrub species *Betula Nana* and *Salix reticulate,* as well as mosses within the *Sphagnum* species group. Spectral similarity between land cover classes can be seen Figure 3.9.

The overall accuracy of the Hyperion classification is 78 %, with a kappa value of 0.73 (Figure 4.4). The final classification map can be seen in Figure 4.5. The classes having the lowest users and producers accuracies are the Shrubs (41% and 64%) and Heath (68% and 50%).

In the producers accuracy analysis, the Heath class has the lowest accuracy (50%). As shown in the error matrix, Heath is primarily being confused with Shrubs. While Heath and Shrubs have very similar spectral signature (Figure 3.12) in all bands except pca137-145, what may have been more problematic was the fact that in areas where these two classes are in close proximity, the spatial resolution of the Hyperion sensor was creating mixed pixels. Heath mounds primarily occur on areas that are slightly higher than the surrounding land cover. This elevation change would eventually lead to water tracks being established around the outer edges of the Heath mounds. As with a lot of the water tracks that were viewed from the helicopter or visited within the

research area, it is reasonable to assume that the dwarf and/ or tall shrubs would eventually become established within these water tracks (Figure 4.6).

The WGT class (63%) was being confused with the Barren, Heath, and Water classes. The confusion between WGT and Water was easily understood because there will always be a water/saturation component in WGT. The WGT's confusion with the Barren and Heath class is more problematic. As seen in the Hyperion spectral profile (Figure 3.12), WGT, Barren and Heath have very different spectral signatures within the pca135-142 band making it less likely that these classes would cross classified. The only reasonable explanations for these misclassifications are mixed pixels due to resolution, altered pixel values brought about by the focal analysis, and analyst error.

The very low users accuracy of the Shrubs class (41%) was primarily believed to be caused by issues just mentioned within the producers accuracy; spectral similarities and mixed pixels caused by spatial resolution. However, for the users accuracy the additional confusion with the MAT and MNT classes produced even lower accuracies. Many of the earlier Arctic land cover classifications were beset with classification errors caused by the similarities within the MNT and MAT classes (Walker et al., 1982, 1991, 1994, 2002; Stine et al., 2010; Pathak, 2010; Muller et al., 1998). This study seems to be affected as well. The misclassification between these three classes could be explained by greater concentrations of the dwarf and/or tall shrubs within some of the MAT and MNT pixels producing higher spectral responses causing them to be more closely aligned to that of the Shrubs. Classes which caused the most classification error for the Shrubs class was Heath (61%), MNT (24%), and MAT (15%).

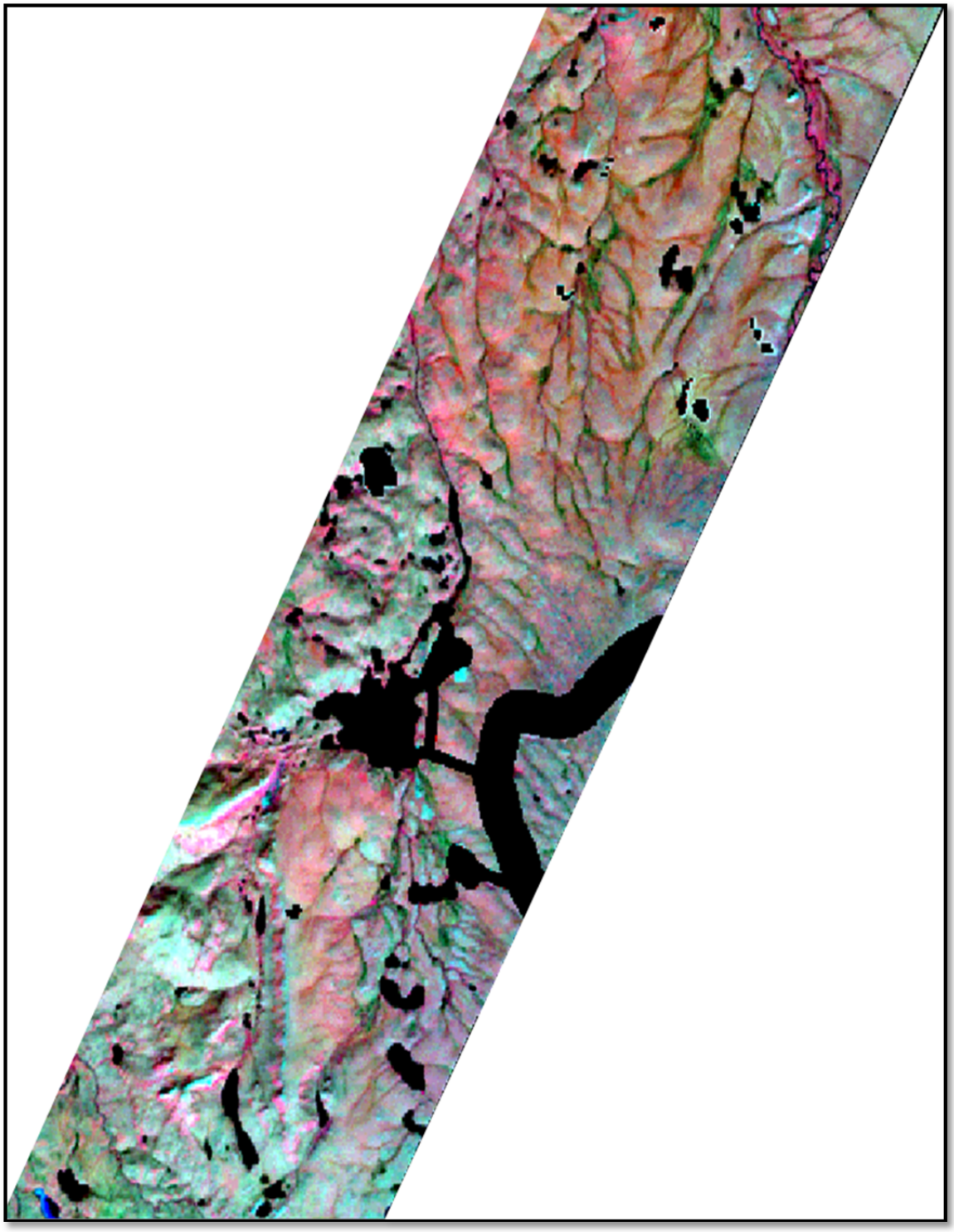

Figure 4.3 2004 Hyperion image.

HYPERION ACCURACY RESULTS

Class Name	Reference Totals	Classified Totals	Number Correct	Producers Accuracy	Users Accuracy
WTR	16	18	16	100.00%	88.89%
WGT	24	16	15	62.50%	93.75%
BARREN	39	42	33	84.62%	78.57%
HEATH	26	19	13	50.00%	68.42%
SHRUBS	14	22	9	64.29%	40.91%
MAT	103	99	85	82.52%	85.86%
MNT	59	63	45	76.27%	71.43%
FEN	10	10	9	90.00%	90.00%
MEADOW	9	11	9	100.00%	81.82%

Overall Classification Accuracy = 78.00%

Conditional Kappa for each Category.

Class Name	Kappa
WTR	0.8826
WGT	0.9321
BARREN	0.7537
HEATH	0.6542
SHRUBS	0.3802
MAT	0.7846
MNT	0.6443
FEN	0.8966
MEADOW	0.8126

Overall Kappa Statistics = 0.7279

Error Matrix

	WTR	WGT	BARREN	HEATH	SHRUBS	MAT	MNT	FEN	MEADOW	Classified Totals	
WTR	16	2	0	0	0	0	0	0	0	18	
WGT	0	15	0	0	0	0	1	0	0	16	
BARREN	0	3	33	0	0	5	0	1	0	42	
HEATH	0	2	0	13	1	0	3	0	0	19	Users
SHRUBS	0	0	0	8	9	2	3	0	0	22	Accuracy
MAT	0	0	5	1	1	85	7	0	0	99	
MNT	0	1	1	3	3	10	45	0	0	63	
FEN	0	0	0	0	0	1	0	9	0	10	
MEADOW	0	1	0	1	0	0	0	0	9	11	
Reference Totals	16	24	39	26	14	103	59	10	9	300	

Producers Accuracy

Figure 4.4 Hyperion accuracy results.

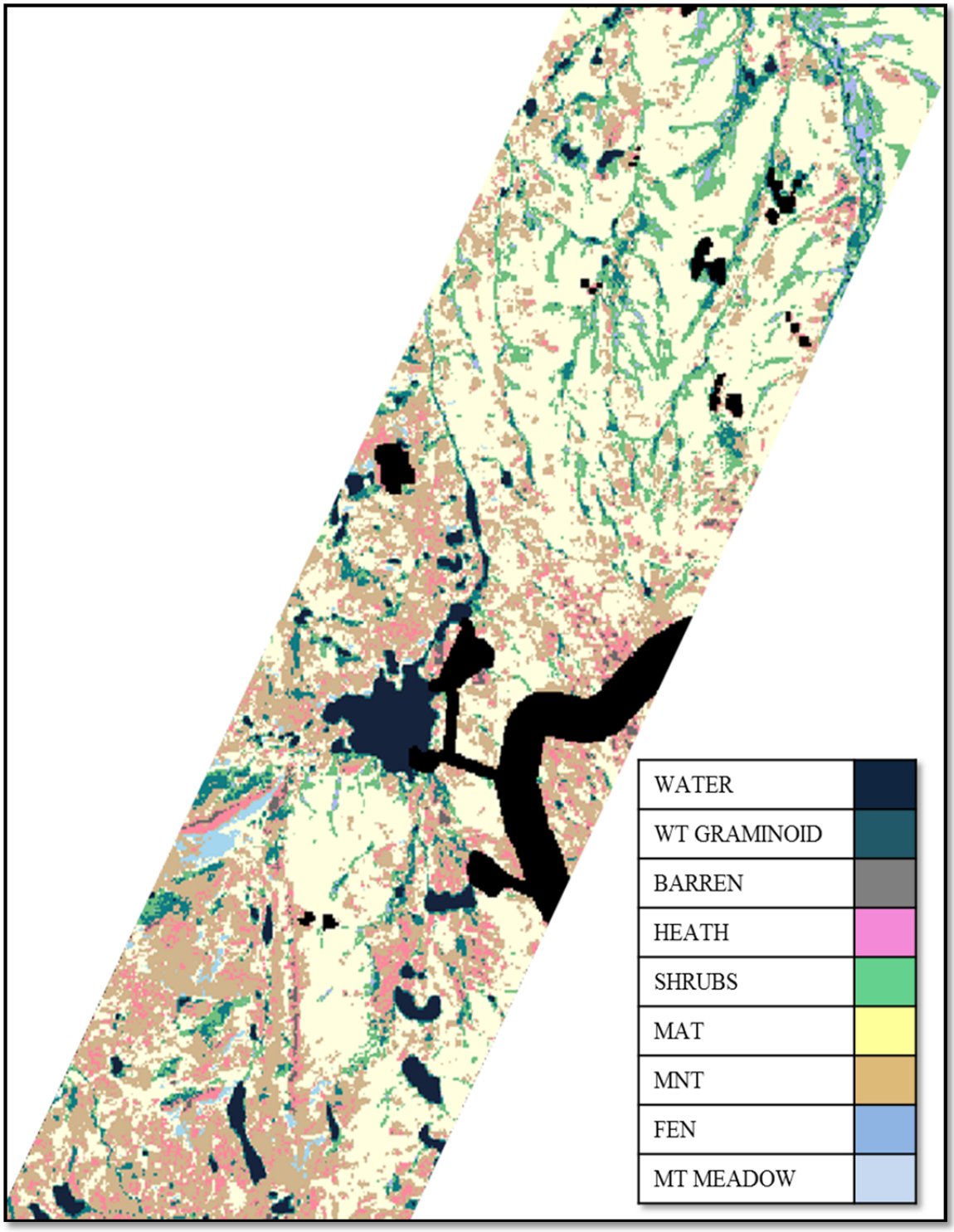

Figure 4.5 Classified 2004 Hyperion image.

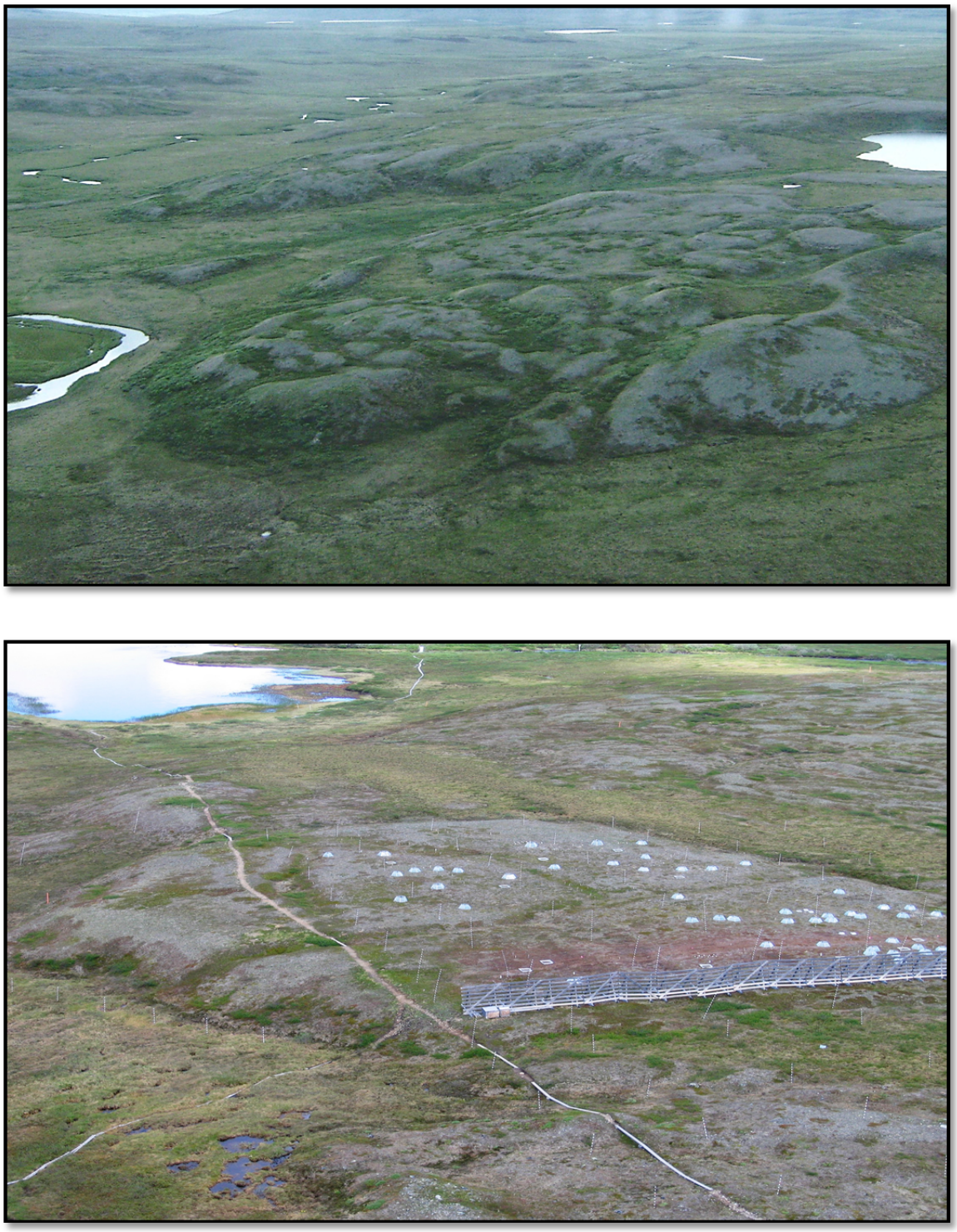

Figure 4.6 Examples of Heath mounds having Shrubs species within the water tracks.

4.2.2 ALI

The ALI classification produced a much higher accuracy rate than did the Hyperion. The overall accuracy for the ALI classification is 87 % with a kappa value of 0.8445 (Figure 4.7). 200 random points were generated to use within the ALI accuracy analysis. The final classification map can be seen in Figure 4.8.

As with the Hyperion image, classifying land cover would seem to be an easy task as the ALI image appears to be so spectrally distinct (Figure 4.9). However, many of the misclassifications within the ALI analysis were due to the same problems experienced within the Hyperion analysis (e.g. spectral similarity, focal analysis, and pixels in shadow). However, the users and producers accuracies don't exhibit any one particular class being mistaken for another repeatedly as in the case of Shrubs and Heath in the Hyperion analysis. Once again, the lowest users and producers accuracy was with the Heath class (63% and 67%). The confusion of the Heath class, as identified by the producers accuracy, with other land cover classes was more easily understood than what was taking place within the users accuracy.

Within the producers accuracy, Heath is being mistaken for the Barren and MNT classes. This can be explained as both the Heath and Barren classes primarily reside within MNT dominated areas. The greatest topography changes occur within the MNT area, and as explained in chapter 1, glacial features are a main factor for land cover classes. It is reasonable to assume that at the top of most of these glacial moraines, kames and eskers, areas of exposed rock, sand and gravel would exist and the changes in elevation would bring changes in land cover. The exposed rock, sand and gravel at the

tops of these hills would be classified as barren. However, over time small vestiges of vegetation would have taken hold which would have produced signatures that more closely resemble Heath. A comparison between the classification maps of the Hyperion and ALI is shown in Figure 4.12.

Within the users analysis, Barren (64%) and Heath (63%) are once again being confused with MNT for the same reasons listed above. However, the Heath was being confused with the MAT class which does not make sense. This is where I believe the root of this classification error is the focal analysis procedure.

ALI ACCURACY RESULTS

Class Name	Reference Totals	Classified Totals	Number Correct	Producers Accuracy	Users Accuracy
WTR	13	14	13	100.00%	92.86%
WGT	14	12	11	78.57%	91.67%
BARREN	10	14	9	90.00%	64.29%
HEATH	15	16	10	66.67%	62.50%
SHRUBS	25	25	22	88.00%	88.00%
MAT	59	57	85	88.14%	91.23%
MNT	39	40	45	89.74%	87.50%
FEN	14	12	12	85.71%	100.00%
MEADOW	11	10	10	90.91%	100.00%
	Overall Classification Accuracy =			**87.00%**	

Conditional Kappa for each Category.

Class Name	Kappa
WTR	0.8826
WGT	0.9321
BARREN	0.7537
HEATH	0.6542
SHRUBS	0.3802
MAT	0.7846
MNT	0.6443
FEN	0.8966
MEADOW	0.8126

Overall Kappa Statistics = 0.8445

Error Matrix

	WTR	WGT	BARREN	HEATH	SHRUBS	MAT	MNT	FEN	MEADOW	Classified Totals	
WTR	13	1	0	0	0	0	0	0	0	14	
WGT	0	11	0	0	1	0	0	0	0	12	
BARREN	0	1	9	2	0	0	1	1	0	14	
HEATH	0	0	1	10	0	3	2	0	0	16	Users
SHRUBS	0	1	0	0	22	1	0	1	0	25	Accuracy
MAT	0	0	0	1	2	52	1	0	1	57	
MNT	0	0	0	2	0	3	35	0	0	40	
FEN	0	0	0	0	0	0	0	12	0	12	
MEADOW	0	0	0	0	0	0	0	0	10	10	
Reference Totals	13	14	10	15	25	59	39	14	11	200	
	Producers Accuracy										

Figure 4.7 Accuracy totals for the ALI classification.

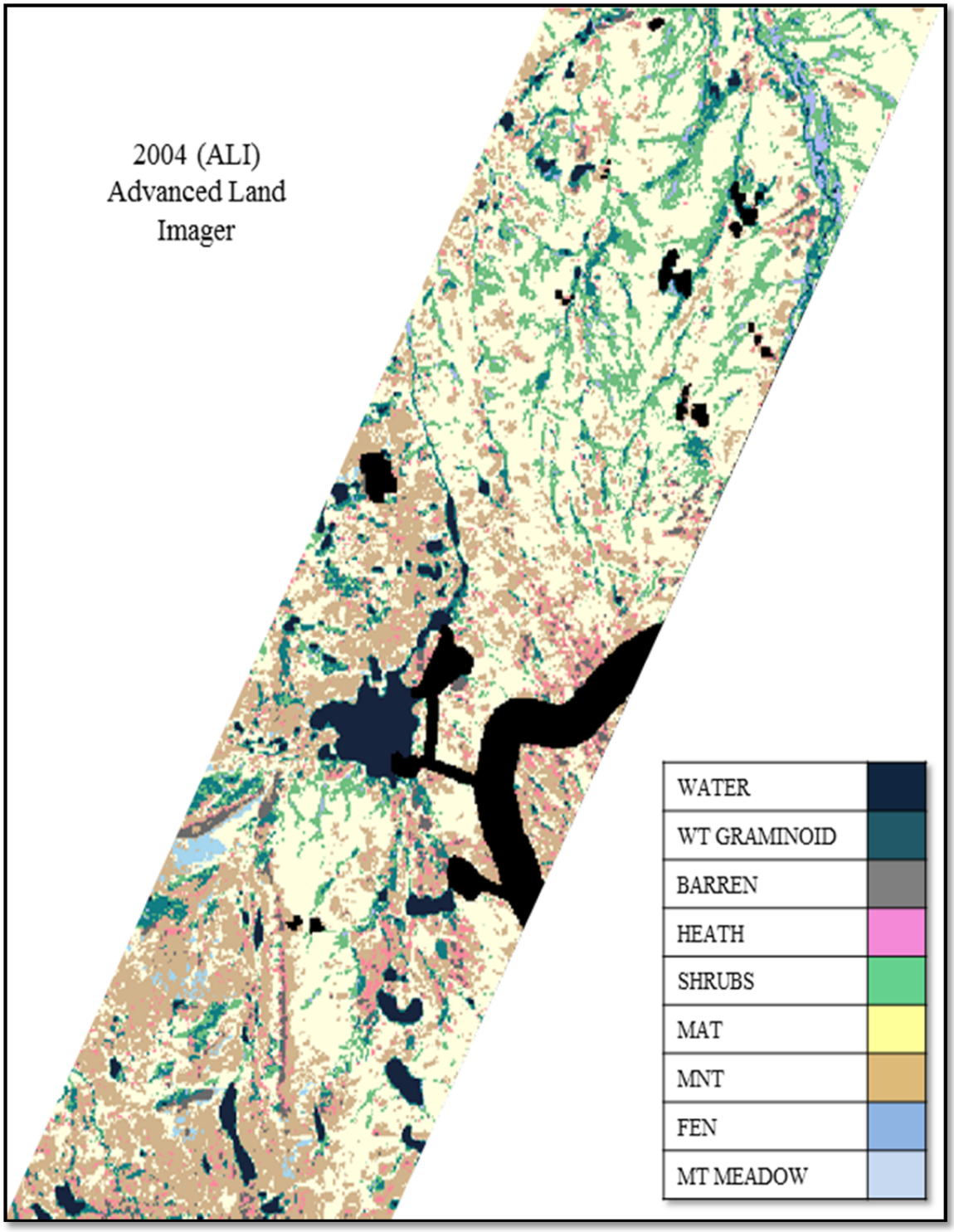

Figure 4.8 Classified 2004 ALI image.

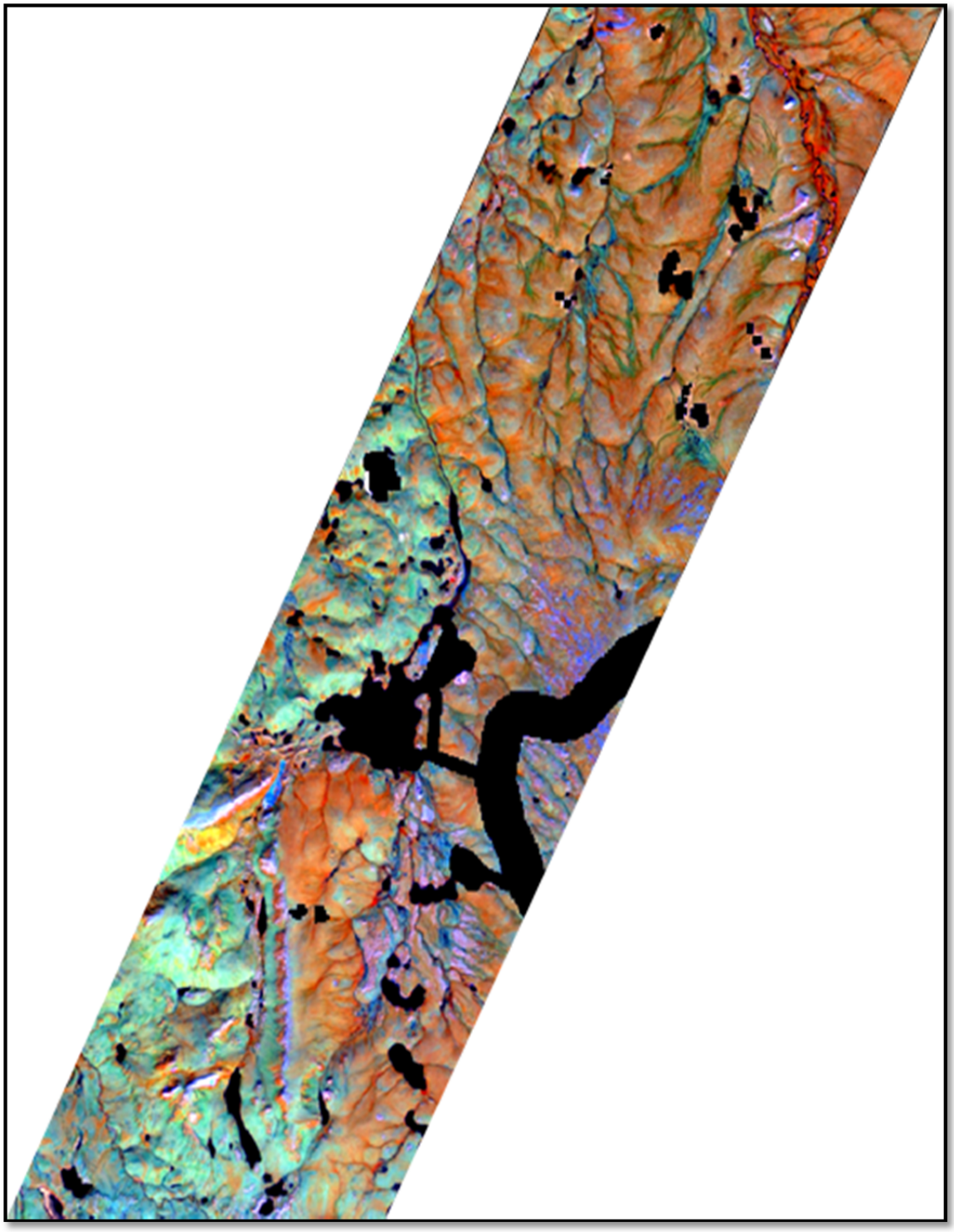

Figure 4.9 ALI image using study bands 5-7-9 for RGB.

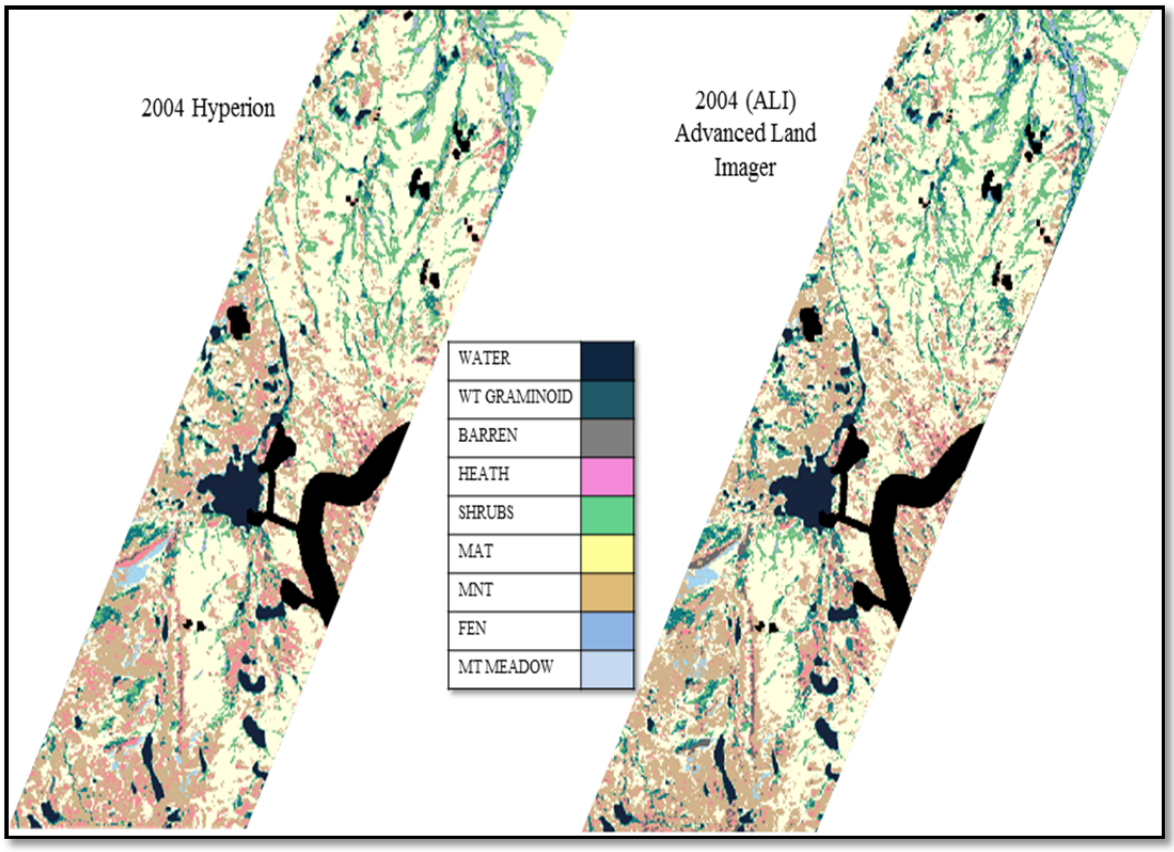

Figure 4.10 Classifications of Hyperion and ALI images.

4.2.3 Landsat TM and ETM+ and SPOT 5

Classification accuracies of the Arctic biome derived from Landsat TM and ETM+ and SPOT Satellites commonly range between 71% and 87% (Muller et al., 1998; Stine et al., 2009; Fleming, 1988; Stow et al., 2000; Tommervik et al., 2003; Goodenough et al., 2003; Walker et al., 1994; Schneider et al., 2009; Fraser et al., 2012). While fewer classes usually produce higher classification accuracies (Rees, 2001), there are instances where higher accuracies have been achieved due to the limited scope of the research (Leverington, 2010, 90%) or where distinct spectral, spatial or textural characteristics are indicative of class identification (Frohn et al., 2005, 98%).

For the past three decades, Arctic researchers have utilized the Landsat TM and ETM+ sensors to create land cover maps within the Arctic. Although an accuracy assessment was not performed, Walker and Acevedo (1987) created a land cover classification map of the Beechey Point Quadrangle, Alaska. However, Jorgenson et al. (1994) achieved overall classification accuracies of 63% to 78% for land-cover maps of the coastal plain of ANWR. An overall classification accuracy of 84% was achieved by The Pacific Meridian Resources (1995) for the western portion of the National Petroleum Reserve. Tommervick et al. (2003) achieved overall accuracies of 75% to 83% on seven different land-cover maps created to monitor and identify changes within the land cover occurring from 1970 to 2000. Brown and Young (2006) achieved a classification accuracy of 77% while researching classification techniques for the delineation of Arctic lakes and ponds. Schneider (2006) was able to achieve accuracies of 78% while researching methane emissions of Arctic vegetation within the Arctic Lena Delta region.

Some of the newer research has been utilizing the higher spatial resolution SPOT sensors to create land cover maps.

SPOT sensors have been utilized to create land cover maps at local levels within the Arctic. Stine et al. (2009) using a hybrid classification technique produced an overall accuracy rating of 76% while, depending on the watershed, Pathak (2010) was able to achieve classification accuracies ranging from 82% to 95%. Nordkvist et al. (2011) combined the SPOT 4 sensor with airborne laser scanner (ALS) data and achieved an overall classification accuracy of 81%. Beck et al. (2011) used statistical models based on decision trees to classify SPOT 5 and IKONOS images (2.5m and 1m spatial resolution) by first turning the image data into binary maps of shrub presence or absence. Regression models utilizing the binary classification maps were then performed on the much larger spatial resolution Landsat (30m) images in order to predict areas of shrub and tall shrub presence achieving an $r^2 = 0.72$ for total shrub cover and an $r^2 = 0.63$ for tall shrub cover.

CHAPTER V

CONCLUSIONS AND FUTURE RESEARCH

The results of this analysis show that the overall accuracies for both the Hyperion and ALI land cover classifications (78% and 87%) were well within the acceptable range of classification accuracies that have previously been derived from Landsat TM and ETM+ sensors (around 65% to 85%). For most regional Arctic land cover studies, both the Hyperion and ALI sensors would be an acceptable replacement for the retiring Landsat satellites. The ALI, however, with its ability to be pan-sharpened to 10m, would have the capacity to map at similar scales and with similar accuracy as the SPOT HRV sensor.

The Hyperion and ALI imagery produced similar classification accuracies of earlier Landsat TM and ETM+ and SPOT 5 studies, although those studies utilized a multitude of complicated classification techniques and/or reduced the size of the research area or scale in order to increase their accuracies (Jia, 2003; Stow et al., 2003; Rees et al., 2003; Tommercik et al., 2003; Frohn et al., 2005; Theau et al., 2005; Schneider et al., 2009; Cullen et al., 2006; Stine et al., 2010; Pathak, 2010; Chadhruri; 2008). This raises the question: If those advanced techniques were applied to the Hyperion and ALI imagery, how improved could the classification accuracy rates become?

Misclassifications due to mixed pixels could possibly be resolved by incorporating hybrid classification techniques such as decision trees, rule-based, and

artificial networks into the classification process. For example, incorporating a rule that defined Heath as having dryer soils and located on elevated topography may eliminate the misclassifications between Heath and Shrubs that were common within this study. The ALI accuracies would increase simply by pan sharpening the image before classification. The ALI data includes one band that has been acquired at 10 meters spatial resolution. The pan sharpening process divides the larger cells' spectral data by that of the smaller cells' spatial extent, and, in the case of ALI, creates 9 separate cells with individual BVs. This would make the ALI imagery more comparable to that of the SPOT in its resolution and accuracies. Even greater accuracies could be accomplished by using the combination of pan sharpened imagery with the additional hybrid classification techniques previously discussed.

5.1 Research Objectives

1. *Compare the optical properties of various Arctic land covers as derived from four satellite sensors: the multispectral ETM+, the advanced multispectral ALI, the hyperspectral Hyperion, and the multispectral (high resolution) SPOT.*

The Infrared and Red wavelengths of the EMR spectrum are the primary regions that correspond to vegetation health and abundance. As the Hyperion, ALI, SPOT, Landsat TM and ETM+ images were constructed of data from basically the same areas of the spectrum it makes sense that there would be similarities between spectral signatures (Chadhrui, 2008; Pathak, 2010; Muller et al., 1998). Band 7 of the ALI image is the only band that corresponds to an area outside the others. It lies in a region that is between the

MIR and FIR band wavelengths of the other sensors. However, it was not one of the primary wavelengths selected by the step-wise discrimination model. The area of the EMR spectrum that was most discriminating for both the Hyperion and ALI image was the MIR region, 1517nm – 1749nm (Figures 3.9 and 3.10).

2. Identify sensor producing highest accuracy land cover classification.

Of the sensors explored within this research, the high radiometric and spatial resolution of the SPOT 5 sensor has outperformed the other sensors helping Arctic land cover classification accuracies rise into the 80^{th} and 90^{th} percentile (Pathak, 2010; Allard, 2003; Muller et al., 1998). However, this accuracy comes at the cost of an ever decreasing study extent or scale. On the other hand, this research has shown that the ALI sensor is able to provide high classification accuracy while still maintaining larger expanses. An additional benefit to using the ALI sensor is the possibility of deriving a greater number of land cover classes.

3. Identify land cover type most and least accurately recognized.

Within this study, the land cover types most accurately recognized were the Water and Mt. Meadow classes. These finding agreed with other studies that also included both of these classes (Stine et al., 2010; Pathak, 2010). The red and NIR wavelengths are absorbed in water, thus giving it a low reflectance signature within those wavelengths, making it fairly easy to recognize. The Mt. Meadow class reflects extremely high within the red and NIR wavelengths due to the high chlorophyll levels within vegetation species belonging to its assemblage (Pathak, 2010).

The Shrubs class, utilizing the Hyperion sensor, obtained the lowest classification accuracy, on average ~52%. This was a surprisingly different outcome from other studies where the confusion between MNT and MAT assemblages made them the prime candidates for misclassification (Stine et al., 2010; Pathak, 2010; Muller et al; 1998; Walker et al., 1994, 2001). However, within this study the Hyperion sensor accurately classified MAT and MNT classes on average ~ 85% and 74% of the time respectively. The ALI sensor performed at even greater accuracies.

4. Provide methodology to utilize Hyperion and ALI imagery in Arctic studies.

Research within the Arctic faces intrinsic difficulties primarily due to its remoteness and climate and obtaining ground truth data can be difficult and expensive. This study provides methodology to derive an image for final classification from an

image that only contains pixels where ground truthing has been accomplished, and/or pixels correspond to those GTPs upon initial classification.

5. *Provide further discourse on the evolution of data continuity between Landsat and EO-1 sensors and previous Arctic studies.*

Arctic researchers can be assured that future data obtained by the E-01 sensors will seamlessly integrate into any historical, ongoing, or future research. They have outperformed the TM and ETM+ sensors consistently (Thekenbail et al., 2003 & 2004; Pu et al., 2005; and Goodenough, 2003). While both the Hyperion and ALI imagery can be constructed to match the characteristics of Landsat TM and ETM+ imagery, it's the ALI sensor that has the capability for its imagery to be modified so that it can match much of the SPOT imagery characteristics (Goodenough et al., 2003; Chen et al., 2003). Researchers who want to use the Hyperion data because of the hyperspectral capabilities may have to spend more time than anticipated on data preparation as the techniques and methodologies for processing Hyperion data are much more complex than with Landsat imagery. The technological learning curve is not as steep with ALI data, and the ALI data can be enhanced so that it rivals the more expensive and spatially limiting SPOT dataset.

5.2 Future Research

Future steps for this research would be to first compare the classification accuracies between a pan-sharpened and regular ALI image (Figure 5.1). Secondly, the pan-sharpened ALI's classification accuracy should be compared to that of not only the SPOT sensor, but to the IKONOS sensor as well. While this is the first study concerning the Hyperion sensors usefulness within the Tundra landscape, research has already taken place using the ALI sensor to study dissolved organic matter (DOM) levels within Arctic lakes (Kutser et al., 2005).

The ALI is the best sensor to replace the long serving Landsat TM sensor for most Arctic studies. However, if the accuracies for the Hyperion image were increased, using the Hyperion sensor in future thermokarst and carbon studies could prove extremely interesting.

The importance of monitoring the changes taking place within the Arctic cannot be overstated. The correlation between changes within the Arctic and the changes throughout the rest of the world has been well documented (Walsh et al., 1991; Gorham et al., 1991; Mack et al., 2004; Callaghan et al., 2004; Sitch et al., 2007). Through the sciences of remote sensing and GIS, a myriad of information can be recorded and analyzed. As the Arctic's spring and summer seasonal windows open and close quickly, sensors aboard satellites and other platforms need to document the changes that are taking place. The significance of this study to Arctic researchers (and all researchers that have depended on the free or inexpensive Landsat imagery) is that a viable option is

available. The EO-1 sensors are able to meet the challenges that are associated with Arctic research.

Remote sensing and Geographic Information Science provide new techniques and methodologies in which to combine imagery with field work. This powerful combination is a way to record, save and analyze changes within the Arctic environment. Because of the specific problems Arctic researchers face concerning remoteness, quickly changing weather, and/or satellite-to-earth angles, obtaining pristine imagery and extensive field data are often difficult to obtain. Imagery, however, has the capability to reveal a plethora of information that can lead to many research opportunities that might have been previously unknown or thought too difficult to perform. Arctic vegetation heterogeneity, or patchiness, has caused problems for past land cover classification studies when using medium to small resolution imagery (Schneider et al., 2009; Muller et al., 1999; Walker et al., 1989). The findings from this dissertation encourage Arctic scientists to add the Hyperion and ALI sensors into the cache of tools they use every day to gather information about an environment.

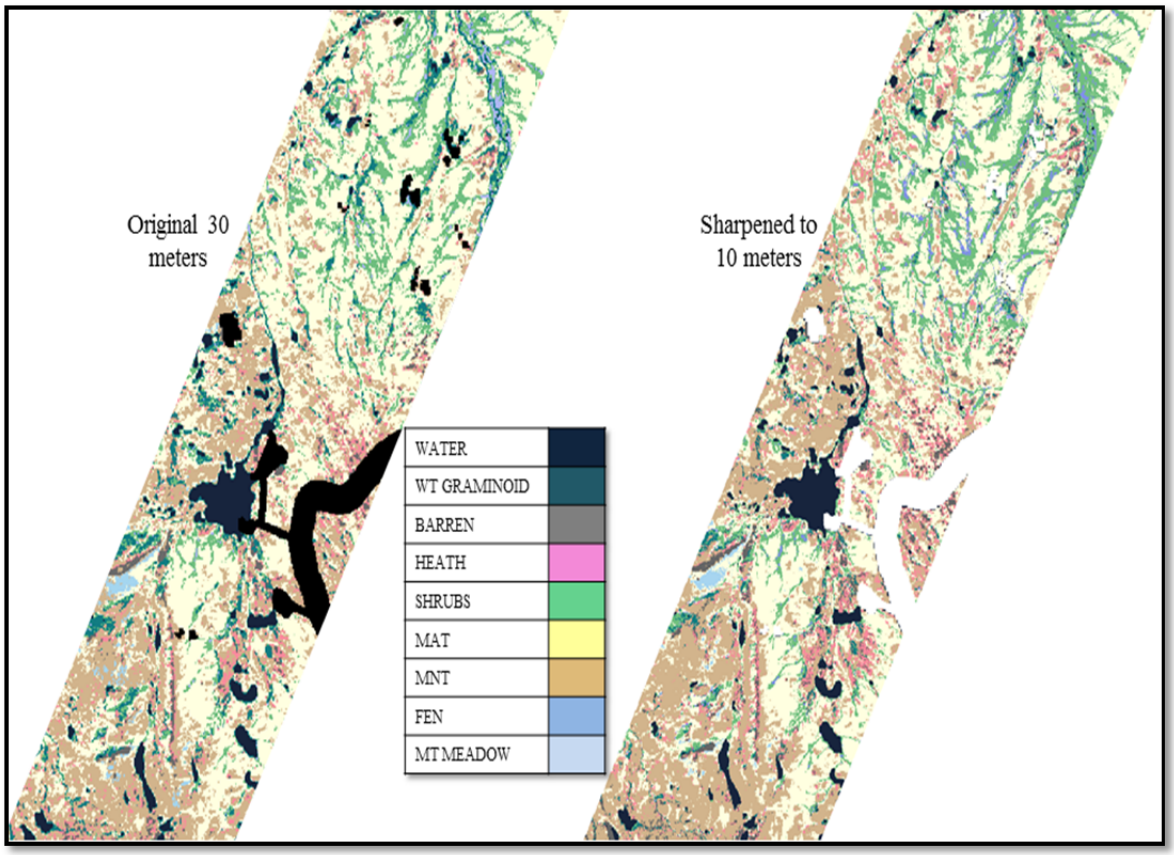

Figure 5.1 Classifications of original and pan-sharpened ALI images.

REFERENCES

AMAP. 1991. Arctic Monitoring and Assessment Programme, 1991. http://www.amap.no/AboutAMAP/GeoCov.htm. Accessed 06/02/2012.

Auerbach, N., Walker, D., and Bochheim, J. 1997. Land cover map of the Kuparuk River basin, Alaska. Institute of Arctic and Alpine Research, University of Colorado, Boulder, Colorado, USA.

Auerbach, N., Walker, M., and Walker, D. 1997. Effects of roadside disturbance on substrate and vegetation properties in Arctic tundra. *Ecological Applications*. V7:1, 218-235.

Beck, R. 2003. EO-1 User Guide, V2.3. http://eo1.usgs.gov/documents/-EO1userguidev2pt320030715UC.pdf. Accessed 02/10/2009.

Beck, P., Horning, N., Goet z, S., Loranty, M., and Tape, K. 2011. Shrub cover on the North Slope of Alaska: a circa 2000 baseline map. *Arctic, AntArctic, and Alpine Research*, V43:3, 335-363.

Belchansky, G.I.; Ovchinikov, G.K.; Kozlenko, N.N.; Douglas, D.C. 1995. Assessment of dependence between SAR data focusing parameters and tundra habitat classification. *Geoscience and Remote Sensing Symposium, 1995. IGARSS '95. 'Quantitative Remote Sensing for Science and Applications', International* , V1: 219-221.

Bishop, P., Shroder, J., Hickman, B. and Copland, L. 1998. Scale dependant analysis of satellite imagery for characterization of glacier surfaces in the Karakoram Himalaya. *Geomorphology*. V21:217-232.

Bockheim, J. G., Tarnocai, C. 1998. Recognition of cryoturbation for classifying permafrost affected soils. *Geoderma*. V81:281-293.

Bryant, R., Moran, M.S., McElroy, S.A., Holifield, C., Thome, K.J., Miura, T. and Biggar, S. 2003. Data Continuity of Earth Observing 1 (EO-1) Advanced Land Imager (ALI) and Landsat TM and ETM+. *IEEE Transactions on Geoscience and Remote Sensing*. V41: 6, 1204-1214.

Bruzzone, L., and Persello, C. 2008. A novel approach to the selection of robust and invariant features for classification of hyperspectral images. *International Geoscience and Remote Sensing Society*. V47:9, 3180-3191.

Bunn, A., Goetz, S., Kimball, J., and Zhang, K. 2007. Northern high-latitude ecosystems respond to climate Change. EOS, Transactions, American Geophysical Union. V88: 34, 333-335.

Brown, L. and Young, K. 2006. Assessment of three mapping techniques to delineate lakes and ponds in a Canadian high Arctic wetland complex. *Arctic Institute of North America*. V59:3, 283-293.

Callaghan T.V., L.O. Björn, F.S. Chapin III, Y. Chernov, T.R. Christensen, B. Huntley, R. Ims, M. Johansson, D.J. Riedlinger, S. Jonasson, N. Matveyeva, W. Oechel, N. Panikov, and G. Shaver. 2005. Arctic Tundra and Polar Desert Ecosystems. Chapter 7, p243-352. In: *Arctic Climate Impact Assessment*. Arctic Council, Cambridge University.

Carpenter, G. A., Gjaja, M. N., Gopal, S., & Woodcock, C. E. (1997). ART neural networks for remote sensing: vegetation classification from Landsat TM and terrain data. *IEEE Transactions on Geoscience and Remote Sensing, 35*,308-325.

Canada Center for Remote Sensing. 2008. Tutorial: Fundamentals of Remote Sensing http://www.ccrs.nrcan.gc.ca/resource/tutor/fundam/chapter2/05_e.php. Accessed 8/01/2010.

Chaudhri, D. 2008. Hybrid image classification technique for land-cover mapping in the Arctic Tundra. *Dissertation*.

Chuvieco, E. and Huete, A. 2010. Fundamentals of Satellite Remote Sensing. CRC Press, NY.

Chen, H., Goodenough, D., Dyk, A., McDonald, S., and Han, T. 2003. Change detection with ALI and Landsat satellite data. In Smits, P. and Bruzzone, L. (Eds.), *Analysis of multi-temporal remote sensing images*. 89-97. World Scientific Publishing Company.

Chapin, F., Sturm, M., Serreze, M., McFadden, J., Key, J., Lloyd, A., McGuire, A., Rupp, T., Lynch, A., Schimel, J., Beringer, J., Chapman, W., Epstein, H., Euskirchen, E., Hinzman, L., Jia, G., Ping, C., Tape, K., Thompson, C., Walker, D., and Welker, J. 2005. Role of land-surface changes in Arctic summer warming. *Science,* V310:657-660.

Central Intelligence Agency. 1987. [Graph illustration of the Arctic Region, 1987]. The Perry-Castañeda Library Map Collection: Maps of Polar Regions and Oceans (http://www.lib.utexas.edu/maps/polar.html) Accessed March 26, 2011

Clark, B., Suomalainen, J., and Pellikka, P. 2010. A comparison of methods for the retrieval of surface reflectance factor from multitemporal SPOT HRV, HRVIR, and HRG multispectral satellite imagery. *Canadian Journal of Remote Sensing*. V36:4, 397-411.

Comiso, J. 2003. Warming trends in the Arctic from clear sky satellite observations. *Journal of Climate*. V16, 3498−3510.

Comiso, J. 2006. Arctic warming signals from satellite observations. *Weather*. V61, 70−76.

Cullen, N., Molg, T., Kaser, G., Hussein, K., Steffen, K., and Hardy, D. 2006. Kilimanjaro Glaciers: Recent areal extent from satellite data and new interpretation of observed 20th century retreat rates. *Geophysical Research Letters*. V33 L16502.

Czaplewski, R. 1994. Variance aproximations for assessments of classification accuracy. UDSA Forest Service Research Paper RM-316:1-29

Durieux, L., Kropáček, J., De Grandi, G., and Achard, F. 2007. Object-oriented and textural image classification of the Siberia GBFM radar mosaic combined with MERIS imagery for continental scale land cover mapping. *International Journal of Remote Sensing.* V28:18, 4175-4182.

Epstein, H., Baringer, J., Gould, W., Loyd, A., Thompson, C., Chapin III, F., Michaelson, G., Ping, C. Rupp, T., and Walker, D., 2004. The nature of spatial transitions in the Arctic. *Journal of Biogeography*. V31:1917-1933.

Epstein, H., Calef, M., Walker, M., Chapin III, F., Starfield, A.2004. Detecting changes in Arctic tundra plant communities in response to warming over decadal time scales. *Global Change Biology*. V10:1325-1334.

ERDAS Inc. Erdas Tour Guide 5th ed. http://www.gis.usu.edu/manuals/labbook/erdas/-manuals/FieldGuide.pdf. Accessed 03/15/09.

ERDAS Inc. Image Spectral Analysis Users Guide, 2008.

Fleming, M.D., and Talbot, S. S. 1982. Landsat assisted classification Togiak National Wildlife Refuge, Alaska. Unpublished report. U.S. Fish and Wildlife Service, Anchorage Alaska.

Fleming, M.D., 1988. An integrated approach for automated cover type mapping of large inaccessible areas in Alaska, *Photogrammetric Engineering & Remote Sensing,* V54:3, 357-362.

Fraser, R., McLennan, D., Ponomarenko, S., Olthof, I. 2012. Image-based predictive ecosystem mapping in Canadian Arctic parks. *International Journal of Applied Earth Observation and Geoinformation*. V14:129-138.

Frohn, R., Hinkel, K., Eisner, W. 2005. Satellite remote sensing classification of thaw lakes and drained thaw lake basins on the North Slope of Alaska. *Remote Sensing of the Environment*. V97: 116-126.

George, T.H., Stringer, W.J., and Baldridge, J.N., 1977. Reindeer range inventory in western Alaska from computer-aided digital classification of Landsat data. *Proceedings of the 11th International Symposium on Remote Sensing of Environment, Environmental Research Institute of Michigan, Anne Arbor*. 671-678.

Goodenough, D., Dyk, A., Niemann, K.O., Pearlman, J.S., Chen, H., Han, T., Murdoch, M., and West, C. 2003. Processing Hyperion and ALI for forest classification. *IEEE Geosciences and Remote Sensing Letters*, V41 6:1321-1331

Google Earth. http://earth.google.com. Accessed 03/15/09.

Gorham, E. 1991. Northern peatlands: role in the carbon cycle and probable response to climatic warming. *Ecological Applications* V1:2,182-195.

Gratto-Trevor, C.L. 1996. Use of Landsat imagery in determining important shorebird habitat in the Outer Makenzie Delta, Northwest Territories. *Arctic Institute of North America*. V49:1, 11-22.

Grosse, G., Shirrmeister, L. and Malthus, T. 2006. Application of Landsat-7 satellite data and a DEM for the quantification of thermokarst-affected terrain types in the periglacial Lena-Anabar coastal lowland. *Polar Research*. V25:1, 51-67.

Hall, F. G., Strebel, D. E., Nickeson, J. E., Goetz, S. J. 1991. Radiometric rectification: Toward a common radiometric response among multidate, multisensor images. *Remote Sensing of the Environment*. V35:11-27.

Hamilton, T.D., 1978. Surficial geologic map of the Phillip Smith Mountain s quadrangle, Alaska. U.S. Geological Survey Miscellaneous Field Studies Map MF-879-A, 1:250,000.

Hamilton, T. 2003. Glacial geology of the Toolik Lake and Upper Kuparuk River Regions. Biological papers of the University of Alaska. No.26.

Hershey, A.E., Beaty, S., Fortino, M., Keyse, P., Mou, P., O'Brien, J., Ulseth, A.J., Gettel, G.A., Lienesch, P.W., Luecke, C., McDonald, M.E., Mayer, C.H., Miller, M.C., Richards, C., Schuldt, J.A. and Whalen, S.C., 2006. Effect on landscape factors on fish distribution in Arctic Alaskan lakes. *Freshwater Biology*. V51:39-55.

Hese, S., Grosse, G. and Pocking, S. 2010. Object based thermokarst lake change mapping as part of the ESA data user element (DUE) permafrost. *The* I*nternational Archives of the Photogrammetry, Remote Sensing and Spatial Information Sciences*. V38:4/C7.

Hirtle, H. and Rencz, A. 2003. The relationship between spectral reflectance and dissolved organic carbon in lake water: Kejimkujik National Park, Nova Scotia, Canada. *International Journal of Remote Sensing*. V24:5, 953-957.

Hope, A., Boynton, W. and Stow, D. 2003. Interannual growth dynamics of vegetation in the Kuparuk River watershed, Alaska based on the Normalized Difference Vegetation Index. *International Journal of Remote Sensing*. V24:17, 3413-3425.

Hope, A., Engstrom, D. R., & Stow, D. A. 2005. Relationship between AVHRR surface temperature and NDVI in Arctic tundra ecosystems. *International Journal of Remote Sensing*. V26:1771−1776.

Hope, A., Kimball, J., and Stow, D. 1993. The relationship between tussock tundra spectral reflectance properties, and biomass and vegetation composition. *International Journal of Remote Sensing*. V14:1861−1874.

Huete, A., Miura, T., Kim, H., and Yoshioka, H. 2003 Use of EO-1 Hyperion data for inter-sensor calibration of vegetation indices. *IEEE Transactions on Geoscience and remote Sensing.* V41:6, 1268-1276.

Jensen, J.R., Rutchey, K., Koch, M.S. and Narumalani, S., 1995. Inland wetland change detection in the everglades water conservation area 2A using a time series of normalized remotely sensed data. *Photogrammetric Engineering & Remote Sensing*. V61:2,199-209.

Jensen, J. 2004. Remote Sensing of the Environment: An Earth Resource Perspective. Prentice-Hall Inc, NJ.

Jensen, J. 2005. Introductory Digital Image Processing: A Remote Sensing Perspective. . Pearson Prentice Hall, NJ.

Jia, G., and Epstein, H. 2003. Greening of Alaska, 1981 – 2001. *Geophysical Research Letters*. V30:20, 2067.

Jia, G., and Epstein, H., 2004. Controls over intra-seasonal dynamics of AVHRR NDVI for the Arctic tundra in northern Alaska. *International Journal of Remote Sensing*. V25:9, 1547-1564.

Jia, G.J., Epstein, H.E., and Walker, D. 2002. Spatial characteristics of AVHRR-NDVI along latitudinal transects in northern Alaska. *Journal of Vegetation Science*. V13:315-326.

Jia, G.J., Epstein, H.E., and Walker, D. 2006. Spatial heterogeneity of tundra vegetation response to recent temperature changes. *Global Change Biology*. V12:42-55.

Jorgenson, J.C., P.E. Joria, T.R. McCabe, B.E. Reitz, M.K. Raynolds, M. Emers, and M.A. Williams, 1994. *User's Guide for the Land-Cover Mop of the Coastal Plain of the Arctic National Wildlife Refuge,* U.S. Dept. of the Interior, U.S. Fish and Wildlife Service Region 7, Anchorage, Alaska, 46 p

Jolliffe, I.T., 2002. Principle Componnent Analysis, 2ed. Springer. New York, NY.

Kutser, T. Pierson, D., Kallio, K. Reinart, A. and Sobek, S. 2005. Mapping lake CDOM by satellite remote sensing. *Remote Sensing of the Environment*. V94: 4, 535-540.

Kutzbach, L., Wagner, D., and Pfeiffer, E. 2004. Effect of microrelief and vegetation on methane emission from wet polygonal tundra, Lena Delta, Northern Siberia. *Biogeochemistry*, V69: 341-362.

Kuzera, K. and Pontius, R. 2008. Importance of Matrix construction for multiple-resolution categorical map comparison. *GIScience and Remote Sensing*. V45:3, 249-274.

Kimball, J., Zhao, M., McDonald, K., and Running, S. 2006. Satellite remote sensing of terrestrial net primary production for the Pan-Arctic basin and Alaska. Mitigation and Adaptation Strategies for Global Change. V11:783-804

Laidler, G. and Treitz, P. 2003. Biophysical remote sensing of Arctic environments. *Progress in Physical Geography*. V27:1, 44-68.

Laidler, G., Treitz, P., and Atkinson, D. 2008. Remote sensing of Arctic vegetation: Relations between the NDVI, spatial resolution and vegetation cover on Boothia Peninsula, Nunavut. *Arctic*. V61:1, 1-13.

Leverington, D. 2010. Discrimination of sedimentary lithologies using Hyperion and Landsat Thematic Mapper data: a case study at Melville Island, Canadian High Arctic. *International Journal of Remote Sensing*. V31:1,233-260.

Lillesand, T., Kiefer, R., and Chipman, J. 2008. Remote Sensing and Image Interpretation. 6th ed. John Wiley and Sons, Inc.

Liew, S.C., Chang, C.W., and Lim, K.H. 2002. Hyperspectral land cover classification of EO-1 Hyperion data by principal component analysis and pixel unmixing. *IEEE Geoscience and Remote Sensing Symposium*. V6:3111-3113.

Liston, G., Mcfadden, J., Sturm, M. and Pielke, R. 2002. Modelled changes in Arctic tundra snow, energy and moisture fluxes due to increased shrubs. *Global Change Biology*. V8:1, 17-32.

Mack, M., Schuur, E., Bret-Harte, S., Shaver, G., and Chapin III, F. 2004. Ecosystem carbon storage in Arctic tundra reduced by long-term nutrient fertilization. *Nature* V431:440-443.

Markon, C. 1994. Identification of tundra land cover near Teshekpuk Lake, Alaska using SPOT satellite data. *Arctic Institute of North America.*

Markon, C., Fleming, M., and Binnian, E. 1995. Characteristics of vegetation phenology over the Alaskan landscape using AVHRR time series data. *Polar Record*. V31:177, 179-190.

McDonald, M., Hershey, A., and Miller, M. 1996. Global warming impacts on lake trout in Arctic lakes. *Limnology and Oceanography*. V41:5, 1102-1108.

Mooney, H. 1991. Biological response to climate change: An agenda for research. *Ecological Applications*. V1:2, 112-117.

Moore, T.E, Wallace, W.K, Bird, K.J., Karl, S.M., Mull, C.G., and Dillion, J.T. 1994. *The Geology of Alaska*, within *The Geology of North America,* Vol. G-1. The Geological Society of America Inc., Co.

Miller, J.M., 1973. Environmental surveys in Alaska based on ERTS data. In Third Earth Resources Technology Satellite Symposium, Summary of Results, NASA Goddard Space Flight Center, Washington, District of Columbia. V2: 13-40.

Muller, S., Racoviteanu, A., and Walker, D. 1999. Landsat BS-derived land-cover map of northern Alaska: extrapolation methods and a comparison with photo-interpreted and AVHRR-derived maps. *International Journal of Remote Sensing*. V20:15, 2921-2946.

Muller, S.V., Walker, D.A., Nelson, F.E., Auerbach, N.A., Bockheim, J.G., Guyer, S., and Sherba, D., 1998. Accuracy assessment of a land-cover map of the Kuparuk River Basin, Alaska: Considerations for Remote Regions. *Photogrammetric Engineering & Remote Sensing*. V64:6, 619-628.

Munger, C. 2007. Spatial and temporal patterns of vegetation, terrain, and greenness in the Toolik Lake and Upper Kuparuk River region. (Unpublished thesis) University of Alaska Fairbanks.

Murphy, T. B., Dean, N., Raftery, A. E. 2008. Variable selection and updating in model-based discriminant analysis for high-dimensional data. Technical report no. 536, Department of Statistics, University of Washington

Nagendra, H., and Gadgil, M. 1999. Biodiversity assessment at multiple scales: Linking remotely sensed data with field information. *Proceedings of the National Academy of Sciences* USA, V96:16, 9154–9158.

National Aeronautics and Space Administration. Retrieved 9/2/11. http://landsat.gsfc.nasa.gov/ Last updated on Friday, September 2, 2011

National Aeronautics and Space Administration, Science Mission Directorate. 2010. *Introduction to The Electromagnetic Spectrum*. Retrieved April 01, 2011, from Mission:Science website: http://missionscience.nasa.gov/ems/01_intro.html

Nelson, T., Wilson, H.G., Boots, B., and Wulder, M.A., 2005. Use of ordinal conversion for radiometric normalization and change detection. *International Journal of Remote Sensing*. V26:3, 535-541.

Nikolakopoulos, Skianis, G. and Vaiopoulos, D. 2007. EO-1 Hyperion and ALI bands simulation to Landsat 7 ETM+ bands and comparison. *Proceedings of SPIE*. V6742:1-11.

Nordkvist, K., Nystrom, M., Reese, H., Holmgren, J., and Olsson, H. 2011. Vegetation classification in the Swedish sub-Arctic using a combination of optical satellite images and airborne laser scanner data. Proceedings from the *11th International Conference on LIDAR Applications for Assessing Forest Ecosystems.* 16-20 Oct. Hobart, Australia.

NSDIC, 1976. National Snow and Ice Data Center. http://nsidc.org/Arcticmet/basics/-Arctic_definition.html. Accessed 07/22/2012.

Oldeland, J., Dorigo, W., Lieckfield, L., Lucieer, A., and Jurgens, N. 2010. Combining vegetation indices, constrained ordination and fuzzy classification for mapping semi-natural vegetation units from hyperspectral imagery. *Remote Sensing of the Environment*. V114:1155-1166.

Olthof, I. and Latifovic, R. 2007. Short term response of Arctic vegetation NDVI to temperature anomolies. *International Journal of Remote Sensing*. 28:21, 4823-4840.

Pacific Meridian Resources. 1995. National petroleum reserve Alaska land-cover inventory: Phase 1 Western NPRA, Final Report, Pacific Meridian Resources Sacramento, Ca. 30p.

Pathak, P., 2010. Geospatial Analysis of Lake and Landscape Interactions within the Toolik Lake Region, North Slope of Alaska. (Unpublished doctoral dissertation) University of North Carolina Greensboro, Greensboro NC.

Ray, Peter. 2006. Personal communication.

Raynolds, M., Walker, D., and Maier, H. 2006. NDVI patterns and phytomass distribution in the circumpolar Arctic. *Remote Sensing of Environment*. V102: 271−281.

Rees, W. Williams, M. and Vitebsky, P. 2003. Mapping land cover change in a reindeer herding area of the Russian Arctic using Landsat TM and ETM+ imagery and indigenous knowledge. *Remote Sensing of the Environment*. V85:441-452.

Rees, W. 2001. Physical principles of remote sensing. 2nd ed. Cambridge University Press, UK.

Riedel, S., Epstein, H., Walker, D., Richardson, D., Calef, M. Edwards, E. and Moody, A. 2005. Spatial and temporal heterogeneity of vegetation properties among four Tundra plant communities at Ivotuk, Alaska, U.S.A. *Arctic, AntArctic, and Alpine Research*. V37:1, 25-33.

Rizvi, I.A., and Mohan, B.K., 2010. Improving accuracy of object based supervised image classification using cloud basis function neural network for high resolution satellite images. *International Journal of Image processing*. V4:4,342-353.

Serpico, S. and Moser, G. 2006. Extraction of spectral channels from hyperspectral images for classification purposes. *IEEE Transactions on Geoscience and Remote Sensing*. V45:2, 484-495.

Schneider, J., Grosse, G., Wagner, D. 2009. Land cover classification of tundra environments in the Arctic Lena Delta based on Landsat 7 ETM+ data and its application for upscaling of methane emissions. *Remote Sensing of the Environment*. V113: 380-391.

Shiklomanov, N. and Nelson, F. 2002. Active layer mapping at regional scales: A 13 year spatial time series for the Kuparuk Region, North-Central Alaska. *Permafrost and Periglacial Processes*. 13:219-230.

Shipper, M., Walker, D., Auerbach, N., and Lewis, B. 1995.Biomass and leaf-area index maps derived from SPOT images for Toolik Lake and Imnavait Creed areas, Alaska. *Polar Record*. V31:147-154.

Spjelkavik, S. 1995. A satellite-based map compared to a traditional vegetation map of Arctic vegetation in the Ny-Alesund area, Svalbard. *Polar Record*. V31:177, 257-269.

Steinberg, D. Goetz, S. and Hyer, E. 2006. Validation of MODIS Fpar products in Boreal Forests of Alaska. *IEEE Transactions on Geoscience and Remote Sensing*. V44:7, 1818-1828.

Stehman, S. 2009. Sampling designs for accuracy assessment of land cover. *International Journal of Remote Sensing*. V30:20, 5243-5272.

Stehman, S. 1997. Estimating standard errors of accuracy assessment statistics under cluster sampling. *Remote Sensing of the Environment*. V60:258-269.

Stine R., Chaudhuri, D., Ray, P., Pathak, P., Hall-Brown, M. 2010. Comparing Image Classification Techniques for Arctic Tundra Land Cover, Toolik Lake, Alaska. *GIScience and Remote Sensing.*V47:1, 78-98.

Stow, D., Daeschner, S., Boynton, W., and Hope, A., 2000. Arctic tundra functional types by classification of single date and AVHRR bi-weekly NDVI composite datasets. *International Journal of Remote Sensing*. V21:8, 1773-1779.

Stow, D., Daeschner, S., Hope, A., Douglas, D., Peterson, A., Myneni, R., Zhou, L., and Oechel, W. 2003. Variability of the Seasonally Integrated Normalized Difference Vegetation Index Across the North Slope of Alaska in the 1990s. *International Journal of Remote Sensing*. V24:5, 1111-1117.

Stow, D., Hope, A., and George, T. 1993. Reflectance characteristics of Arctic tundra vegetation from airborne radiometry. *International Journal of Remote Sensing.* V14:1239−1244.

Stow, D., Hope, A., McGuire, D., Verbyla, D., Gamon, J., Huemmrich, F., Houston, S., Racine, C., Sturm, M., Tape, K., Hinzman, L., Yoshikawa, K., Tweedie, C., Noyle, B., Silapaswan, C, Douglas, D., Griffith,B., Jia, G., Epstein, H., Walker, D. Daeschner, S., Peterson, A., Zhou, L., and Myneni, R., 2004. Remote sensing of vegetation and land-cover change in Arctic Tundra Ecosystems. *Remote Sensing of Environment*. V89: 231-308.

Sturm, M., McFadden, J. P., Liston, G. E., Chapin, F. S. I., Racine, C. H., and Holmgren, J. 2001. Snow-shrub interactions in Arctic tundra: A hypothesis with climatic implications. *Journal of Climate*. V14:336−344.

Sturm, M., Racine, C., and Tape, K., 2001. Increasing Shrub abundance in the Arctic. *Nature*. V411: 546-547.

Sturm, M., Schimel, J., Michaelson, G., Welker, J., Oberbauer, S., Liston, G., Fahnestock, J., and Romanovsky, V. 2005. Winter biological processes could help convert Arctic tundra to shrubland. *BioScience.* V55:1, 17-26.

Tape, K., Sturm, M., and Racine, C. 2006. The evidence for shrub expansion in Northern Alaska and the Pan-Arctic. *Global Change Biology*. V12:686-702.

Theau,J., Peddle, D., and Duguay, C. 2005. Mapping lichen in a caribou habitat of Northern Quebec, Canada, using an enhancement-classification method and spectral mixture analysis. *Remote Sensing of the Environment*. V94:2,232-243.

Thenkabail, P., Enclona, E. Ashton, M. Legg, C. and De Dieu, M. 2004. Hyperion, IKONOS, ALI and ETM+ sensors in the study of African rainforests. *Remote Sensing of the Environment*. V90:23-43.

Tommervik, H., Hogda, K., Solheim, I. 2003. Monitoring vegetation changes in Pasvik (Norway) and Pechenga in Kola Peninsula (Russia) using multitemporal Landsat BS/TM data. *Remote Sensing of the Environment.*V85:3, 370-388.

Tucker, C., Pinzon, J., and Brown, M. 2004. Global Inventory Modeling and Mapping Studies (GIMB) Satellite Drift Corrected and NOAA-16 incorporated normalized difference vegetation index (NDVI), Monthly 1981–2003. Global Land Cover Facility, University of Maryland.

Tucker, C.J., Slayback, D.A., Pinzon, J.E., Los, S.O., Myneni, R.B. and Taylor, M.G., 2001. Higher northern latitude normalized difference vegetation index and growing season trends from 1982 to 1999. *International Journal of Biometeorology* V45:184-190.

Tutubalina, O.V. and Rees, W.G., 2001. Vegetation degradation in a permafrost region as seen from space: Noril'sk (1961-1999). *Cold Regions Science and Technology*, V32:191-203.

United States Geological Survey (USGS). 2006. Landsat product information and Description. http://edc.usgs.gov/products/satellite/landsat7.php. Accessed 03/16/09. Last updated 08/22/06.

United States Geological Survey (USGS). 2008. EO-1 product information and Description. http://eros.usgs.gov/products/satellite/eo1.php. Accessed 10/30/08. Last updated 08/22/2006.

Ustin, S., and Xiao, Q. 2001. Mapping successional boreal forests in interior central Alaska. International journal of Remote Sensing. V22:6, 1779-1797.

Van Wijk, M., Clemmensen, K., Shaver, G., Williams, M., Callaghan, T., Chapin III, F., Cornelissen, J., Gough, L., Hobbie, S., Jonasson, S., Lee, J., Michelsen, A., Press, M., Richardson, S., and Rueth, H. 2004. Long-term ecosystem level experiments at Toolik Lake, Alaska, and at Abisko, Northern Sweden: generalizations and differences in ecosystem and plant type responses to global change. *Global Change Biology*. V10:1, 105–123.

Verbyla, D. 2008. The greening and browing of Alaska based on 1982-2003 satellite data. *Global Ecology and Biogeography*. V17:547-555.

Vourlitis, G., Verfaillie, J., Oechel, W., Hope, A., Stow, D. and Engstrom, R. Spatial variation in regional CO2 exchange for the Kuparuk River Basin, Alaska over the summer growing season. *Global Change Biology*. V9:930-941.

Walker, D.A and Acevedo, W. 1987. Vegetation and a Landsat-derived cover map of the Beechy Point Quadrangel, Arctic Coastal Plain, Alaska. *CRREL Report,* 87-5, U.S. Army Cold Regions Research and Engineering Laboratory, Hanover, New Hampshire.

Walker, D. and Barry, N., 1991. Toolik Lake permanent vegetation plots: Site factors, soil physical and chemical properties, plant species cover, photographs, and soil descriptions. Department of Energy R4D Program Data report, Joint Facility for Regional Ecosystem Analysis, Institute of Arctic and Alpine Research, Boulder, CO. Boulder, CO: National Snow and Ice Data Center. Identifier no. ARCSS018.

Walker, D., Bockheim, J., Chapin, F., Eugster, W., Nelson, F., and Ping, C. 2001. Calcium-rich tundra, wildlife, and the Mammoth Steppe. *Quaternary Science Reviews*. V20:149−163.

Walker, D., Epstein, H., Jia, J., Balser, A., Copass, C., and Edwards, E. 2003. Phytomass, LAI, and NDVI in northern Alaska: Relationships to summer warmth, soil pH, plant functional types, and extrapolation to the circumpolar Arctic. *Journal of Geophysical Research- Atmospheres*. V108:8169

Walker, D. Everett, K., Acevedo, W., Gaydos, L., Brown, J., and Webber, P. 1982. Landsat-assisted environmental mapping in the Arctic National Wildlife Refuge, Alaska. *CREL Report 82-27*. U.S. Army Cold Regions and Engineering Laboratory, Hanover, NH.

Walker, D., Gould, W., Maier, H., and Reynolds, M. 2002. The Circumpolar Arctic Vegetation Map: AVHRR-derived base maps, environmental controls, and integrated mapping procedures. *International Journal of Remote Sensing*. V23:21, 4551- 4570.

Walker, D., Halfpenny, J. Walker, M. and Wessman, C. 1993. Long-term studies of snow-vegetation interactions: A hierarchic geographic information system helps examine links between species distributions and regional patterns of greenness. *BioScience*. V43:5, 287-301.

Walker, D., Raynolds, M., Daniels, F., Einarsson, E., Elvebakk, A., and Gould, W. 2005. The Circumpolar Arctic Vegetation Map. *Journal of Vegetation Science*. V16:267−282

Walker, D. and Walker, M. 1991. History and pattern of disturbance in Alaskan Arctic Terrestrial Ecosystems: A hierarchical approach to analyzing landscape change. *The Journal of Applied Ecology*, V28:1, 244-276.

Walker, M., Walker, D., and Auerbach, N. 1994. Plant Communities of a tussock tundra landscape in the Brooks Range Foothills, Alaska. *Journal of Vegetation Science*. V5: 843-866.

Walker, M.,Wahren, C., Hollister, R., Henry, G., Ahlquist, L., and Alatalo, J. 2006. Plant community responses to experimental warming across the tundra biome. *Proceedings of the National Academy of Sciences*. V103:1342−1346.

Walsh, J. 1991. The Arctic as a bellwether. *Nature*. V352: 19-20.

Zoran, M. and Stefan, S. 2006. Climatic changes effects on spectral vegetation indices for forested areas analysis from satellite data. Proceedings of the 2nd Environmental Physics Conference, 18-22 Feb. Alexandria, Egypt.

APPENDIX A

SENSORS SPECTRAL COVERAGE SORTED BY WAVELENGTH[7]

ETM Bands	ALI Bands	SPOT	Hyperion Band	Average Wavelength (nm) 10^{-9}	Full Width at Half the Maximum FWHM (nm)	Not Calibrated (X)
			B1	355.59	11.3871	X
			B2	365.76	11.3871	X
			B3	375.94	11.3871	X
			B4	386.11	11.3871	X
			B5	396.29	11.3871	X
			B6	406.46	11.3871	X
			B7	416.64	11.3871	X
			B8	426.82	11.3871	
	B1		B9	436.99	11.3871	
	B1		B10	447.17	11.3871	
B1	B1'		B11	457.34	11.3871	
B1	B1'		B12	467.52	11.3871	
B1	B1'		B13	477.69	11.3871	
B1	B1'		B14	487.87	11.3784	
B1	B1'		B15	498.04	11.3538	
B1	B1'	B1	B16	508.22	11.3133	
B1		B1	B17	518.39	11.2580	
B2	B2	B1	B18	528.57	11.1907	
B2	B2	B1	B19	538.74	11.1119	
B2	B2	B1	B20	548.92	11.0245	
B2	B2	B1	B21	559.09	10.9321	
B2	B2		B22	569.27	10.8368	
B2	B2		B23	579.45	10.7407	
B2	B2		B24	589.62	10.6482	
B2	B2		B25	599.80	10.5607	
B3		B2	B26	609.97	10.4823	
B3		B2	B27	620.15	10.4147	

[7] http://edcsns17.cr.usgs.gov/eo1/sensors/hyperioncoverage
http://www.satimagingcorp.com/satellite-sensors/spot-5.html

ETM Bands	ALI Bands	SPOT	Hyperion Band	Average Wavelength (nm) 10^{-9}	Full Width at Half the Maximum FWHM (nm)	Not Calibrated (X)
B3	B3	B2	B28	630.32	10.3595	
B3	B3	B2	B29	640.50	10.3188	
B3	B3	B2	B30	650.67	10.2942	
B3	B3	B2	B31	660.85	10.2856	
B3	B3	B2	B32	671.02	10.2980	
B3	B3	B2	B33	681.20	10.3349	
B3			B34	691.37	10.3909	
			B35	701.55	10.4592	
			B36	711.72	10.5322	
			B37	721.90	10.6004	
			B38	732.07	10.6562	
			B39	742.25	10.6933	
B4			B40	752.43	10.7058	
B4			B41	762.60	10.7276	
B4	B4		B42	772.78	10.7907	
B4	B4	B3	B43	782.95	10.8833	
B4	B4	B3	B44	793.13	10.9938	
B4	B4	B3	B45	803.30	11.1044	
B4		B3	B46	813.48	11.1980	
B4		B3	B47	823.65	11.2600	
B4		B3	B48	833.83	11.2824	
B4	B4'	B3	B49	844.00	11.2822	
B4	B4'	B3	B71	851.92	11.0457	X
B4	B4'	B3	B50	854.18	11.2816	
B4	B4'	B3	B72	862.01	11.0457	X
B4	B4'	B3	B51	864.35	11.2809	
B4	B4'	B3	B73	872.10	11.0457	X
B4	B4'	B3	B52	874.53	11.2797	
B4	B4'	B3	B74	882.19	11.0457	X
B4	B4'	B3	B53	884.70	11.2782	
B4		B3	B75	892.28	11.0457	X
B4			B54	894.88	11.2771	
			B76	902.36	11.0457	X
			B55	905.05	11.2765	
			B77	912.45	11.0457	
			B56	915.23	11.2756	
			B78	922.54	11.0457	

ETM Bands	ALI Bands	SPOT	Hyperion Band	Average Wavelength (nm) 10^{-9}	Full Width at Half the Maximum FWHM (nm)	Not Calibrated (X)
			B57	925.41	11.2754	
			B79	932.64	11.0457	
			B58	935.58	11.2754	X
			B80	942.73	11.0457	
			B59	945.76	11.2754	X
			B81	952.82	11.0457	
			B60	955.93	11.2754	X
			B82	962.91	11.0457	
			B61	966.11	11.2754	X
			B83	972.99	11.0457	
			B62	976.28	11.2754	X
			B84	983.08	11.0457	
			B63	986.46	11.2754	X
			B85	993.17	11.0457	
			B64	996.63	11.2754	X
			B86	1003.30	11.0457	
			B65	1006.81	11.2754	X
			B87	1013.30	11.0457	
			B66	1016.98	11.2754	X
			B88	1023.40	11.0451	
			B67	1027.16	11.2754	X
			B89	1033.49	11.0423	
			B68	1037.33	11.2754	X
			B90	1043.59	11.0372	
			B69	1047.51	11.2754	X
			B91	1053.69	11.0302	
			B70	1057.68	11.2754	X
			B92	1063.79	11.0218	
			B93	1073.89	11.0122	
			B94	1083.99	11.0013	
			B95	1094.09	10.9871	
			B96	1104.19	10.9732	
			B97	1114.19	10.9572	
			B98	1124.28	10.9418	
			B99	1134.38	10.9248	
			B100	1144.48	10.9065	
			B101	1154.58	10.8884	

ETM Bands	ALI Bands	SPOT	Hyperion Band	Average Wavelength (nm) 10^{-9}	Full Width at Half the Maximum FWHM (nm)	Not Calibrated (X)
			B102	1164.68	10.8696	
			B103	1174.77	10.8513	
			B104	1184.87	10.8335	
			B105	1194.97	10.8154	
	B5'		B106	1205.07	10.7979	
	B5'		B107	1215.17	10.7822	
	B5'		B108	1225.17	10.7663	
	B5'		B109	1235.27	10.7520	
	B5'		B110	1245.36	10.7385	
	B5'		B111	1255.46	10.7270	
	B5'		B112	1265.56	10.7174	
	B5'		B113	1275.66	10.7091	
	B5'		B114	1285.76	10.7022	
	B5'		B115	1295.86	10.6970	
			B116	1305.96	10.6946	
			B117	1316.05	10.6937	
			B118	1326.05	10.6949	
			B119	1336.15	10.6996	
			B120	1346.25	10.7058	
			B121	1356.35	10.7163	
			B122	1366.45	10.7283	
			B123	1376.55	10.7437	
			B124	1386.65	10.7612	
			B125	1396.74	10.7807	
			B126	1406.84	10.8034	
			B127	1416.94	10.8267	
			B128	1426.94	10.8534	
			B129	1437.04	10.8818	
			B130	1447.14	10.9110	
			B131	1457.23	10.9422	
			B132	1467.33	10.9743	
			B133	1477.43	11.0074	
			B134	1487.53	11.0414	
			B135	1497.63	11.0759	
			B136	1507.73	11.1108	
			B137	1517.83	11.1461	

ETM Bands	ALI Bands	SPOT	Hyperion Band	Average Wavelength (nm) 10^{-9}	Full Width at Half the Maximum FWHM (nm)	Not Calibrated (X)
			B138	1527.92	11.1811	
			B139	1537.92	11.2156	
			B140	1548.02	11.2496	
B5	B5	B4	B141	1558.12	11.2826	
B5	B5	B4	B142	1568.22	11.3146	
B5	B5	B4	B143	1578.32	11.3460	
B5	B5	B4	B144	1588.42	11.3753	
B5	B5	B4	B145	1598.51	11.4037	
B5	B5	B4	B146	1608.61	11.4302	
B5	B5	B4	B147	1618.71	11.4538	
B5	B5	B4	B148	1628.81	11.4760	
B5	B5	B4	B149	1638.81	11.4958	
B5	B5	B4	B150	1648.90	11.5133	
B5	B5	B4	B151	1659.00	11.5286	
B5	B5	B4	B152	1669.10	11.5404	
B5	B5	B4	B153	1679.20	11.5505	
B5	B5	B4	B154	1689.30	11.5580	
B5	B5	B4	B155	1699.40	11.5621	
B5	B5	B4	B156	1709.50	11.5634	
B5	B5	B4	B157	1719.60	11.5617	
B5	B5	B4	B158	1729.70	11.5563	
B5	B5	B4	B159	1739.70	11.5477	
B5	B5	B4	B160	1749.79	11.5346	
			B161	1759.89	11.5193	
			B162	1769.99	11.5002	
			B163	1780.09	11.4789	
			B164	1790.19	11.4548	
			B165	1800.29	11.4279	
			B166	1810.38	11.3994	
			B167	1820.48	11.3688	
			B168	1830.58	11.3366	
			B169	1840.58	11.3036	
			B170	1850.68	11.2696	
			B171	1860.78	11.2363	
			B172	1870.87	11.2007	
			B173	1880.98	11.1666	
			B174	1891.07	11.1333	

ETM Bands	ALI Bands	SPOT	Hyperion Band	Average Wavelength (nm) 10^{-9}	Full Width at Half the Maximum FWHM (nm)	Not Calibrated (X)
			B175	1901.17	11.1018	
			B176	1911.27	11.0714	
			B177	1921.37	11.0424	
			B178	1931.47	11.0155	
			B179	1941.57	10.9912	
			B180	1951.57	10.9698	
			B181	1961.66	10.9508	
			B182	1971.76	10.9355	
			B183	1981.86	10.9230	
			B184	1991.96	10.9139	
			B185	2002.06	10.9083	
			B186	2012.15	10.9069	
			B187	2022.25	10.9057	
			B188	2032.35	10.9013	
			B189	2042.45	10.8951	
			B190	2052.45	10.8854	
			B191	2062.55	10.8740	
			B192	2072.65	10.8591	
Band 7	B7		B193	2082.75	10.8429	
Band 7	B7		B194	2092.84	10.8242	
Band 7	B7		B195	2102.94	10.8039	
Band 7	B7		B196	2113.04	10.7820	
Band 7	B7		B197	2123.14	10.7592	
Band 7	B7		B198	2133.24	10.7342	
Band 7	B7		B199	2143.34	10.7092	
Band 7	B7		B200	2153.34	10.6834	
Band 7	B7		B201	2163.43	10.6572	
Band 7	B7		B202	2173.53	10.6312	
Band 7	B7		B203	2183.63	10.6052	
Band 7	B7		B204	2193.73	10.5803	
Band 7	B7		B205	2203.83	10.5560	
Band 7	B7		B206	2213.93	10.5328	
Band 7	B7		B207	2224.03	10.5101	
Band 7	B7		B208	2234.12	10.4904	
Band 7	B7		B209	2244.22	10.4722	
Band 7	B7		B210	2254.22	10.4552	
Band 7	B7		B211	2264.32	10.4408	

ETM Bands	ALI Bands	SPOT	Hyperion Band	Average Wavelength (nm) 10^{-9}	Full Width at Half the Maximum FWHM (nm)	Not Calibrated (X)
Band 7	B7		B212	2274.42	10.4285	
Band 7	B7		B213	2284.52	10.4197	
Band 7	B7		B214	2294.61	10.4129	
Band 7	B7		B215	2304.71	10.4088	
Band 7	B7		B216	2314.81	10.4077	
Band 7	B7		B217	2324.91	10.4077	
Band 7	B7		B218	2335.01	10.4077	
	B7		B219	2345.11	10.4077	
			B220	2355.21	10.4077	
			B221	2365.20	10.4077	
			B222	2375.30	10.4077	
			B223	2385.40	10.4077	
			B224	2395.50	10.4077	
			B225	2405.60	10.4077	X
			B226	2415.70	10.4077	X
			B227	2425.80	10.4077	X
			B228	2435.89	10.4077	X
			B229	2445.99	10.4077	X
			B230	2456.09	10.4077	X
			B231	2466.09	10.4077	X
			B232	2476.19	10.4077	X
			B233	2486.29	10.4077	X
			B234	2496.39	10.4077	X
			B235	2506.48	10.4077	X
			B236	2516.59	10.4077	X
			B237	2526.68	10.4077	X
			B238	2536.78	10.4077	X
			B239	2546.88	10.4077	X
			B240	2556.98	10.4077	X
			B241	2566.98	10.4077	X
			B242	2577.08	10.4077	X

APPENDIX B

VALUES INCLUDED WITHIN RADIOMETRIC CORRECTION ALGORITHMS

Table 1: Earth-Sun Distance in Astronomical Units

Julian Day	Distance	Julian Day	Distance	Julian Day	Distance	Julian Day	Distance	Julian Day	Distance
1	.9832	74	.9945	152	1.0140	227	1.0128	305	.9925
15	.9836	91	.9993	166	1.0158	242	1.0092	319	.9892
32	.9853	106	1.0033	182	1.0167	258	1.0057	335	.9860
46	.9878	121	1.0076	196	1.0165	274	1.0011	349	.9843
60	.9909	135	1.0109	213	1.0149	288	.9972	365	.9833

Table 2: ALI Mean Solar Exo-atmospheric Irradiances (ESUN)

$ESUN_\lambda$ units are in $W/(m^2.\mu m)$	
Band	**ESUN**
b1	1967.6
b1p	1851.8
b2	1837.2
b3	1551.47
b4	1164.53
b4p	957.46
b5	230.03
b5p	451.37
b7	79.61
b8	1747.86

APPENDIX C

FIELD PHOTOS OF VEGETATION ASSEMBLAGES

1. Water

2. Wet Graminoid Tundra Complex

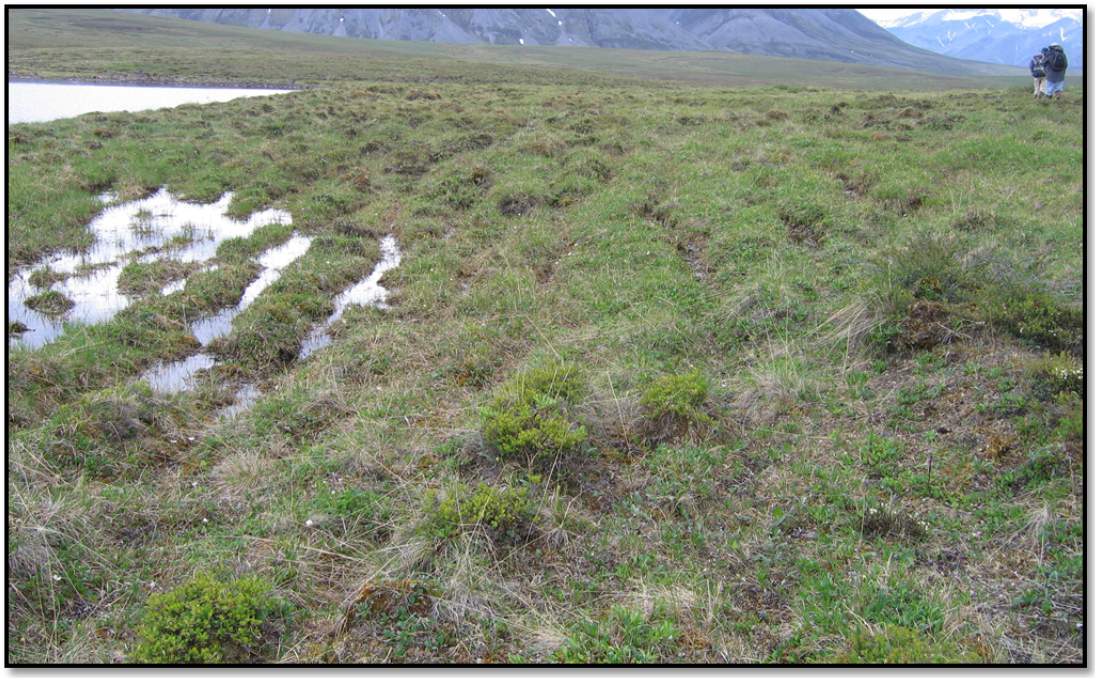

3. Barrens

4. Heath Complex

5. Shrubs Complex

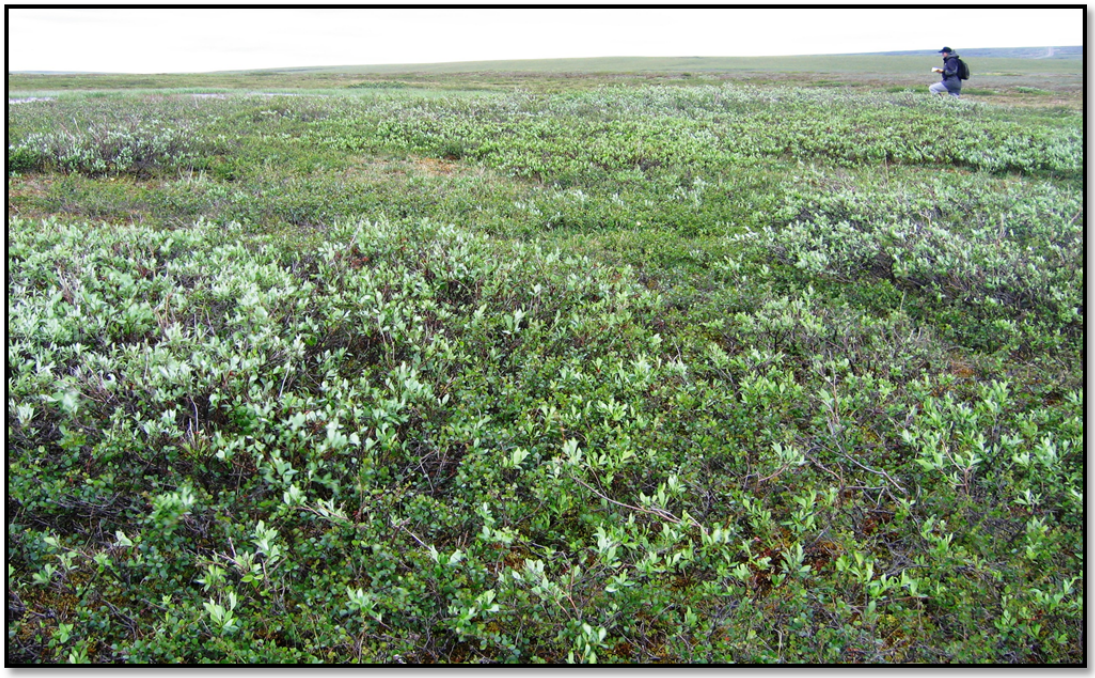

6. Moist Acidic Tussock Tundra Complex

7. Moist Non-Acidic Tussock Tundra Complex

8. Fen Complex

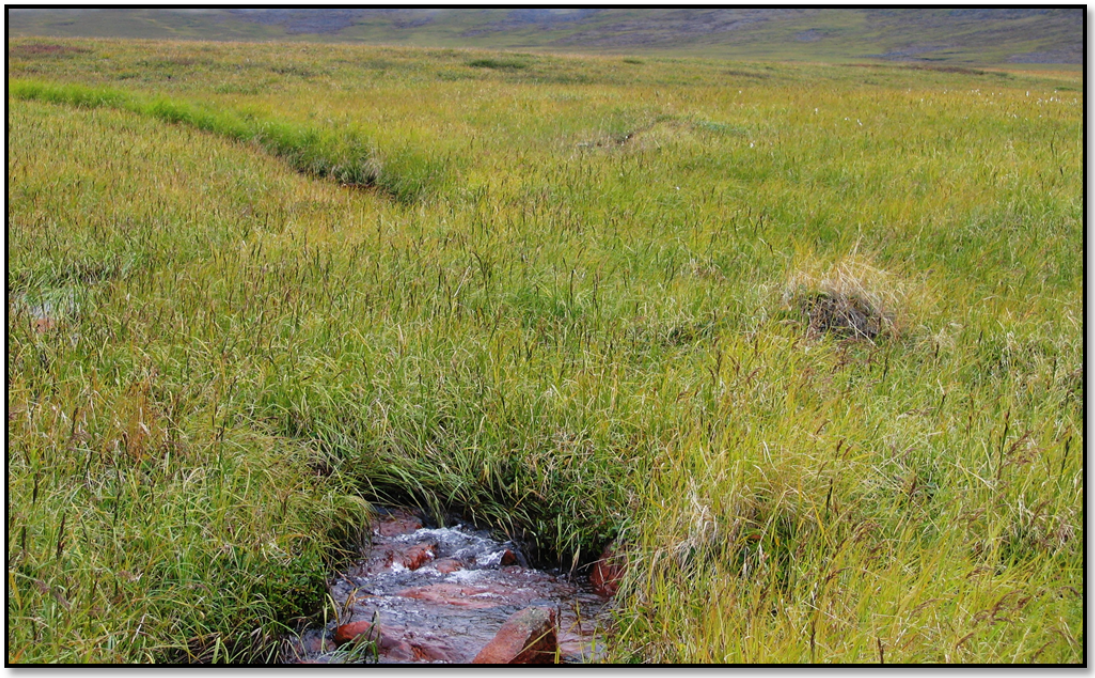

9. Mountain Meadow Complex